CHAPTER 4

Log Editing, Log Prediction and Well Ties

4.1 Principles of Log Editing

A well log can be defined as a highly detailed record of a given geophysical parameter along the confined space of a borehole (Ricker, 2002). Well logging utilizes different tools to assess a whole range of physical properties (e.g. density, sonic velocity, resistivity, natural radioactivity) that are later plotted against the measured depth to be interpreted. Ideally, the aim of a wireline survey is to provide – along the wellbore – a true, repeatable geophysical measurement of the subsurface's formations. When a well is drilled, however, disturbed conditions are created along the borehole. It is a trade-off from obtaining the "ideal" subsurface direct measurement. Due to this fact, environmental conditions in the well (e.g. temperature, pore pressure, mud weight, invasion, etc.) can significantly influence the quality of measurements and should be taken into account (Boyer and Mary, 1997). Inaccurate data values may be caused by the tools themselves as well (e.g. cycle skipping). A perfect measurement would require a tool to be static at every sampling point. It is known though, that tools move as compromises had to be made in order to perform a practical and executable well logging survey (Ricker, 2002). Thus, corrections need to be applied to predict what would be the response given by a measurement taken under perfect conditions.

As a rule of thumb, the petrophysicists focus their attention on making standard corrections for environmental effects on tools related to factors such as stress, mud weight, pore pressure and temperature (Simm and Bacon, 2014). On the other hand, it is responsibility of the geoscientist to identify other problems and correct them according to their need when using well logs on a specific project. For example, bad hole effects (washouts, mud cakes) can result in bad density and sonic readings, which are a common cause of poor well ties; missing sections also quite often occur and normally require empirical relationships to fill data gaps with predictions based on other logs (see

Gardner *et al.* (1974); Faust (1953); Lindseth (1979); Castagna *et al.* (1985)). Therefore, log editing is a paramount element of the well-tie process. For that reason, this chapter addresses the problems with the available well data. A Seismic-to-well tie (synthetic match) is used to verify whether the editing/prediction procedures are acceptable or not.

Tying well logs to seismic data is a mandatory procedure in any inversion project. It provides a time-depth relationship that is used to convert wireline logs from depth into time domain as well as it auxiliates to estimate the source wavelet. Sonic and density logs are used to calculate acoustic impedance and reflectivity logs, which are then convolved with a wavelet to create a synthetic seismogram in a process known as seismic forward modeling (White and Hu, 1998). The synthetic seismogram is then compared to actual seismic traces extracted along the well path. Furthermore, crosscorrelation provides a quantitative measure that can be used to check the quality of well ties. In this context, log editing and log prediction hereafter presented were driven by the purpose of obtaining a better match between seismic and well data.

Following a general overview approaching the reasons why well logs need to be edited before any reservoir characterization study, a summary of the main problems found in the well data used in this study is presented by the following table:

Table 4.1 – Main problems faced during log conditioning step prior well-ties.

Well Name	**Problems**
Kea-1	Many wash-out zones associated to the shales of Upper and Lower Manganui Formations.
Maari-1	Relatively good data, some wash-outs but that does not appear to have compromised well data quality
Maari-2	Mud-cake along most of the section; Relatively spiky logs
Maui-4	Missing sections of density log; Noisy sonic; no Caliper log along most of the well-bore
Moki-1	Most of the section is washed-out; still density and sonic are not greatly affected as local relationships obtained from other wells were applied and matched quite well with the original data

Table 4.1 (Continued)

Well Name	**Problems**
Moki-2A	Noisy data; wash-outs associated to the upper Manganui Fm.
Whio-1	Local wash-outs; spiky data at deeper section, especially at the Mangahewa Fm.

As mentioned earlier, log conditioning, editing, and prediction were carried out on the fly along with the seismic-to-well-tie procedure. Decision making was based mainly in how well the synthetic trace correlates to the seismic data, obviously with the attention to keep velocities and time-depth relations realistic. In order to do that, a series of steps were taken:

- Check-shot correction is applied to adjust the timing of the sonic log with the seismic times from the check-shot data. It is necessary – firstly, because velocities of section above sonic record is unknown; and secondly, due to the fact that normally sonic-log velocities are higher than seismic velocities (check-shot), mainly due to the frequency of the sonic logging experiment;
- De-spiking is performed to attenuate noisy sections of well data. There are several ways to do that (e.g. manually editing, applying filters, replacing sections, blocking), but in this study running average and median filters were used over intervals considered to be noisy, while manually editing was preferred to remove isolated spikes, which are clearly not signal from geology;
- Log predictions were applied in two scenarios: (1) missing sections of density or sonic logs and (2) wash-out zones where the data quality was completely compromised, with the latter occurring especially at the Manganui Formation. Two approaches were tested: local Gardner's relations were used to predict density or sonic missing/bad sections from other wells in an *in gauge* state (caliper value equals to bit size) at those formations. The Emerge module from CGG Geoview HRS software was

also tested. This approach uses multilinear regression to predict missing logs from a multi-wells/multi-logs perspective (Hampson-Russell, 2015).

Since seven wells containing density and sonic logs are available in this study and many procedures are repeated for every well, this chapter will present the main processes applied, decisions taken when editing the well logs; also the final curves as well as the synthetic seismogram over the actual seismic section for each of them.

4.1.1 Sonic Log Calibration

By integrating the sonic log, a time-depth relationship is created. Unfortunately, the sonic log is not normally recorded from the surface, which leaves a section where velocities are unknown. Also, the frequency used by the sonic logging tool is much higher than the frequency of the seismic data. This creates differences between sonic and seismic velocities due to dispersion effects (Al-Chalabi, 2014). In addition, the sonic log may be vulnerable to unfavorable environment conditions along the wellbore. So, due to the fundamental importance of seismic velocities, check-shot or vertical seismic profile (VSP) surveys are carried out in order to gather information about true velocities along the entire well. These surveys utilize acoustic sources in the same frequency range as the seismic data and, unlike the sonic logging in a wellbore environment, the sound waves supposedly travel through the subsurface sampling the rock layers in an undisturbed state (Bisaso, 2011). Thus, ideally, after the calibration process sonic log values are corrected to what they would have been if collected from the surface downwards, at seismic acquisition frequencies and under ideal borehole conditions (Al-Chalabi, 2014).

All the wells used in the present study had either check-shots or VSP's surveys available. A check-shot calibration was therefore applied in order to establish a first link between the sonic log and the seismic data. Applying the check-shot correction adjusts the shallow section, where velocities were unknown, which helps the seismic-to-well tie procedure. It should bring seismic events (in 2-way time, TWT) very close to the right spatial position. After that, only small bulk shifts in time or, sometimes, tiny stretching/squeezing over part of the section should be required to match the reflections events between the synthetic seismogram – produced from density and sonic logs – and actual seismic data. Figure 4.1 presents the check-shot calibration process in the wells Maari-2 and Kea-1, from a VSP and a check-shot survey respectively. Note the differences in the number of sampling points; it is significantly higher in a VSP survey (blue squares along the drift curve). Also note the gray squares in the drift curve of Kea-1; these are possibly wrong check-shot measurements and were left out of the correction procedure.

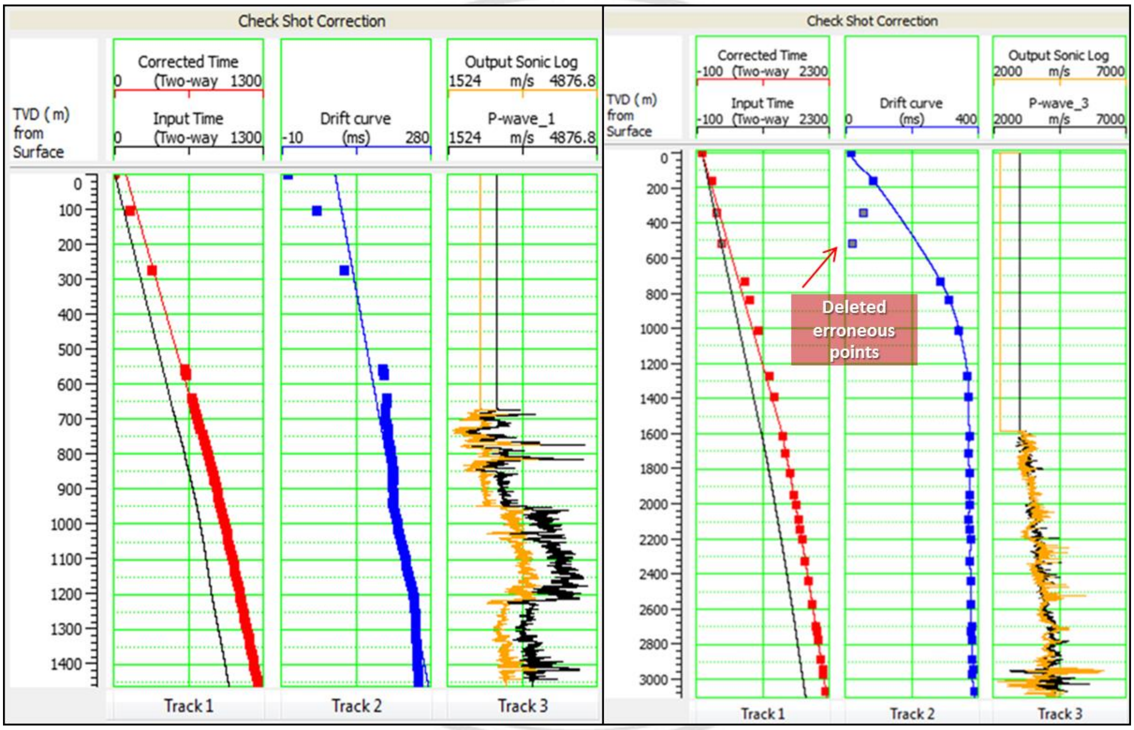

Figure 4.1: Check-shot calibration process in the wells Maari-2 (left hand side) and Kea-1 (right hand side) from a VSP and a check-shot survey, respectively

4.1.2 Spurious Data Identification and de-spiking

A very common way of identifying intervals with potential erroneous data is through a visual inspection at the caliper log. The caliper log measures the variations in borehole diameter along its depth, using two or more articulated arms that are pushed against the borehole wall (Ricker, 2002). When analyzed along with bit-size information, the caliper log is able to indicate zones with unfavorable wellbore conditions, such as wash-outs (caliper > bit-size) and mud-cakes (caliper < bit-size).

Sometimes though, caliper data is not available. Another good quality control is to use cross-plots. Figures 4.2 to 4.5 illustrate application of cross-plots in two situations: in the well Kea-1, where there is a caliper log, and in the well Maui-4, where there is not. In these cross-plots of sonic *vs.* density, areas are created to show that data points diverging from the main cluster correlate to spurious data, which are mainly associated with wash-out zones as evidenced in the Kea-1 well-log data. It is clear that these zones are concentrated especially in shales (high GR values, green data points in the blue area of Figure 4.2) of Manganui Formation (upper and lower), and that such bad borehole conditions strongly affect the density measurements while the sonic trend holds steady (Figure 4.3).

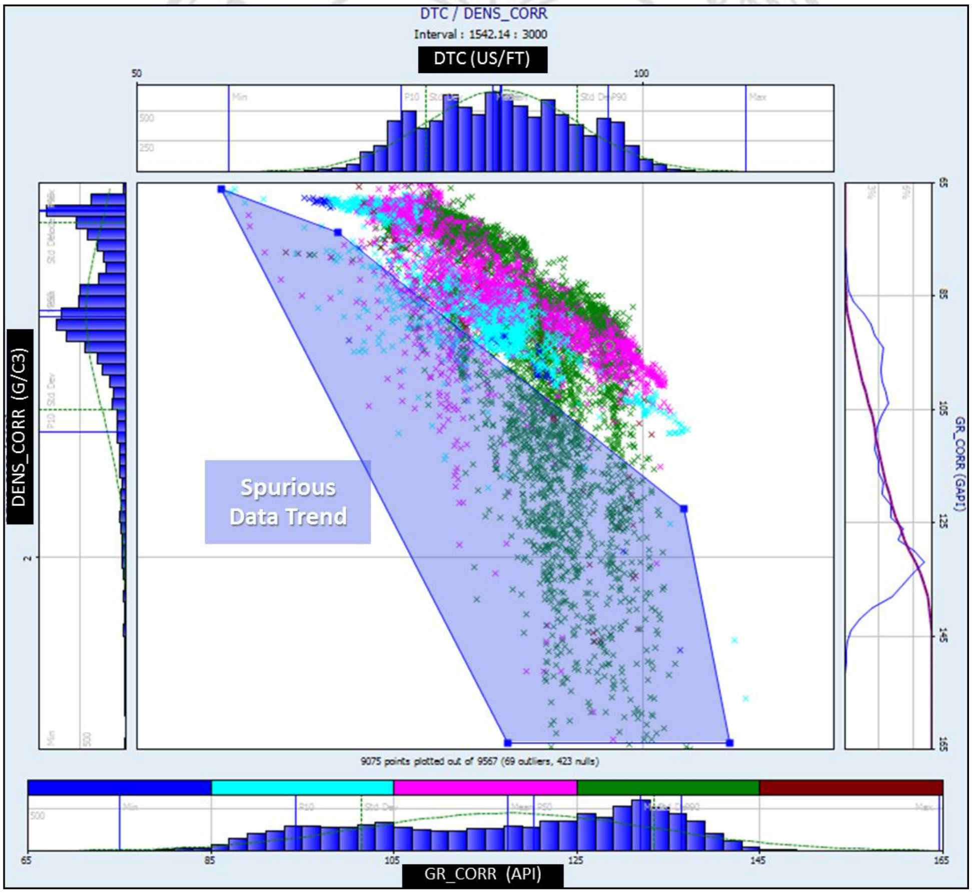

Figure 4.2: Cross-plot of Sonic (DTC) against Density (DENS_CORR) from Kea-1 showing a main cluster and divergent data points. A polygon is created to highlight these divergent data points along the section in the Figure 4.3. Data is colored by Gamma-Ray (GR_CORR)

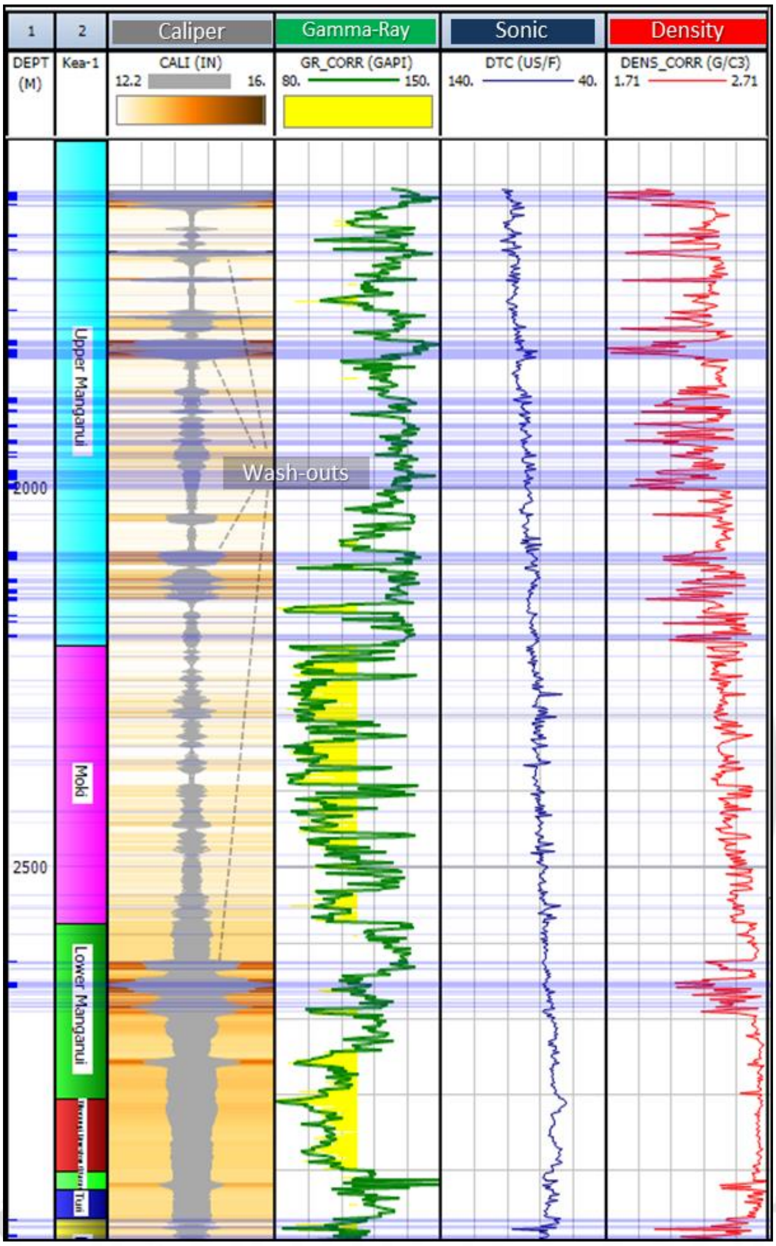

Figure 4.3: Wireline logs along the interval 1542-3000 m (Measured Depth) in the Kea-1 well. Note how the data points included in the polygon of Figure 4.2, highlighted here in blue, correlate well to wash-out zones in the caliper track. Bit size is $12\frac{1}{2}''$

Again, the blue zone containing dispersed data points highlights shales (high Gamma-Ray value) of lower Manganui and Turi Formation. At these zones, the density curve (DENS_CORR) deviates significantly from its general trend and is typically marked by a strong decrease. It suggests that these zones are likely to be affected by wash-outs, as just demonstrated in Kea-1 where caliper confirms wash-out zones preferentially occurring in shales, with density measurements strongly affected while the sonic data quality appears to be unaffected. Besides, these cross-plots help to identify spikes like the ones observed in Moki, Mangahewa and Farewell formations (Figure 4.5) and even infer its probable cause.

There are many reasons for the presence of spikes in well logs. Bisaso (2011) mentions ultra-thin beds leading to constructive interference in the received signal and also wave conversion processes occurring in thin fluid filled fractures as possible causes. But probably the most common one, especially with conventional sonic logs, is known as cycle-skipping. The phenomenon is induced by bad hole conditions that attenuate the sonic signal and, consequently, first arrival amplitudes are too low that the tool is not triggered until later arrivals with higher amplitudes (Simm and Bacon, 2014) . Thus, cycle-skipping is characterized by high slowness readings (i.e. low velocities) that are normally associated to low density measurements due unfavorable borehole conditions. These different trends of spurious data are identified and annotated over the cross-plot presented in Figure 4.4.

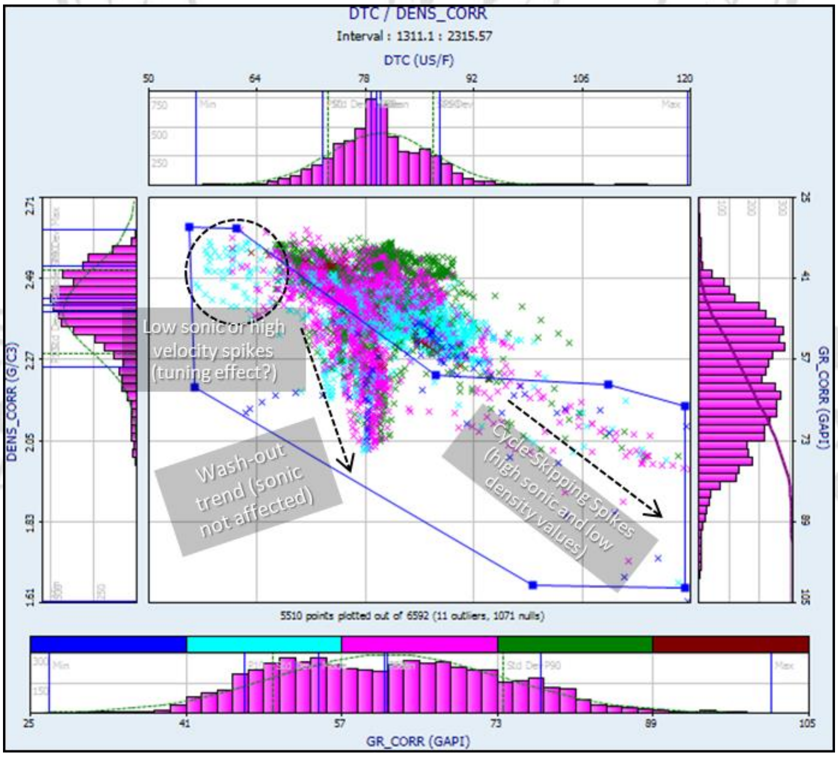

Figure 4.4: Cross-plot of Sonic (DTC) against Density (DENS_CORR) from Maui-4. A blue area is created to highlight potential spurious data along the section in Figure 4.5. Data is colored by Gamma-Ray (GR_CORR)

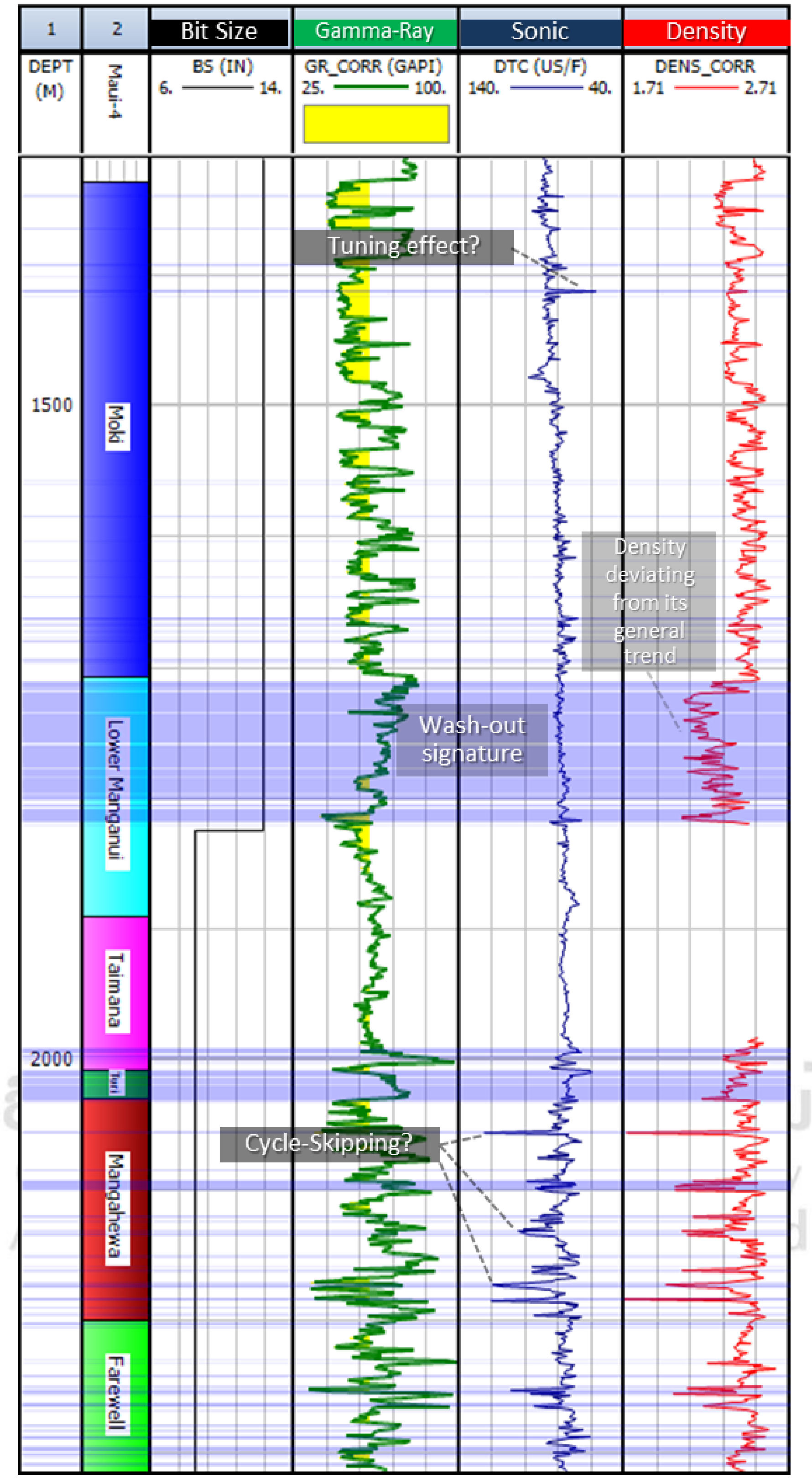

Figure 4.5: Wireline logs along the interval 1311-2315 m (Measured Depth) along the Maui-4 well. Highlighted in blue are the data points included within the blue area of Figure 4.4, showing potential spurious data in the absence of a caliper log

In order to remove undesired spikes from the well data, two approaches were used. A running-average filter and median filters were applied over long noisy/spiky intervals, while manual editing was used to remove isolated spikes. A running-average filter calculates averages in subsets of data defined by a certain window length, moving forward through the data samples after every computation (Smith, 2013). With the median filter, a similar idea is applied, but now the sample value at the center of the operator length is replaced with the median value of the samples within the operator length (Hampson-Russel, 2015). Bianco (2011), for example, uses a similar approach to attenuate spikes in sonic and density curves before calculating synthetic seismograms.

Filters such as running-average and median filter are routinely applied in time-series analysis to smooth out short-term variations (spikes) in the dataset. The two methods have slightly different characteristics. Bisaso (2011) discuss the reasons why using one or the other would be better depending on the case. Special attention should be given to the choice of the window and the operator length when filtering well logs. The reason is that there is an inherent trade-off to each of the methods: large windows/operators will effectively remove the spikes, but at the cost of decreasing vertical resolution; while short windows/operators tend to maintain the original vertical resolution but it might leave or just gently affect the spikes. Figure 4.6 illustrates this trade-off by presenting examples of filtered sonic logs from well Moki-1 applying both methods with different window-length/filter operators. Track 01 (left hand side) shows bit size and caliper log and then Track 02 (central) and Track 03 (right hand size) present original P-wave log and P-wave after running average and median filters, respectively. Three different values of window/operator length were tested: five, ten and twenty samples. The larger the window, the more efficiently it will remove spikes. Although, it might reduce vertical details (resolution) of the sonic log or yet, remove responses (actual signal) that come from the geological medium. So, in this study these filters were cautiously applied to attenuate spikes without compromising the vertical resolution. As it will be shown next, the final curves used to tie the well still contain some spikes, but this alone does not prejudice the quality of well tie.

4.1.3 Log Prediction

Sometimes adequate density and sonic logs are not available. Either it was not recorded in a well or the quality is so bad that it is unusable, so that a substitute predicted curve is required. There are numerous ways of predicting velocity and density curves. Gardner *et al.* (1974), for example, used brine-saturated rocks in a laboratory controlled experiment to determine a relationship between density and velocity. They established the following relation:

$$\rho = aV_p^m \tag{4-1}$$

where ρ is density and V_p is P-wave velocity. The constants a and m are, respectively, 0.31 and 0.25 for density units in g/cm^3 and velocity in m/s. These values are a good approximation for shales, sandstones and carbonates worldwide.

Most of the relationships used in log prediction (e.g. Gardner's, Faust's, Lindseth's) were empirically determined with data from various locations and depths. Establishing local relations for a specific project, therefore, can significantly improve these predictions (Quijada and Stewart, 2007). Local constant values (a and m) need to be obtained in order to modify the general Gardner's equation (Eq. 4-1). This ideally requires wireline logs from wells nearby with the same rock units and similar pressure regime, as emphasized by Simm and Bacon (2014).

As mentioned in Section 4.1, lack of either density or sonic information at specific intervals as well as bad hole conditions resulting in degradation of data quality, particularly in the Manganui Formation (upper an lower), do occur in the wells available for this study and, consequently, had to be dealt with. In order to do that, data from the well Maari-1, which is not compromised by bad hole conditions in these formations (Figure 4.7), was used to create a local Gardner's relationship between density and P-wave velocity. The upper Manganui Formation is described in the well completion report (Halliburton/Shell, 1999) as a massive claystone from 703 to 755m MD and below that, it is claystones interbedded with siltstone and sandstone. The lower Manganui is 227 meters thick in this well and is claystone dominated with interbedded siltstone and sandstone. From the cross-plot in Figure 4.8(a), a power equation was fit to the data points from upper Manganui formation and established local parameters $a = .268$ and $m = .273$ to the Gardner's equation according to the following:

$$\rho = 0.268{V_p}^{0.273} \tag{4-2}$$

with density (ρ) in g/cm^3 and is P-wave velocity (V_p) in m/s.

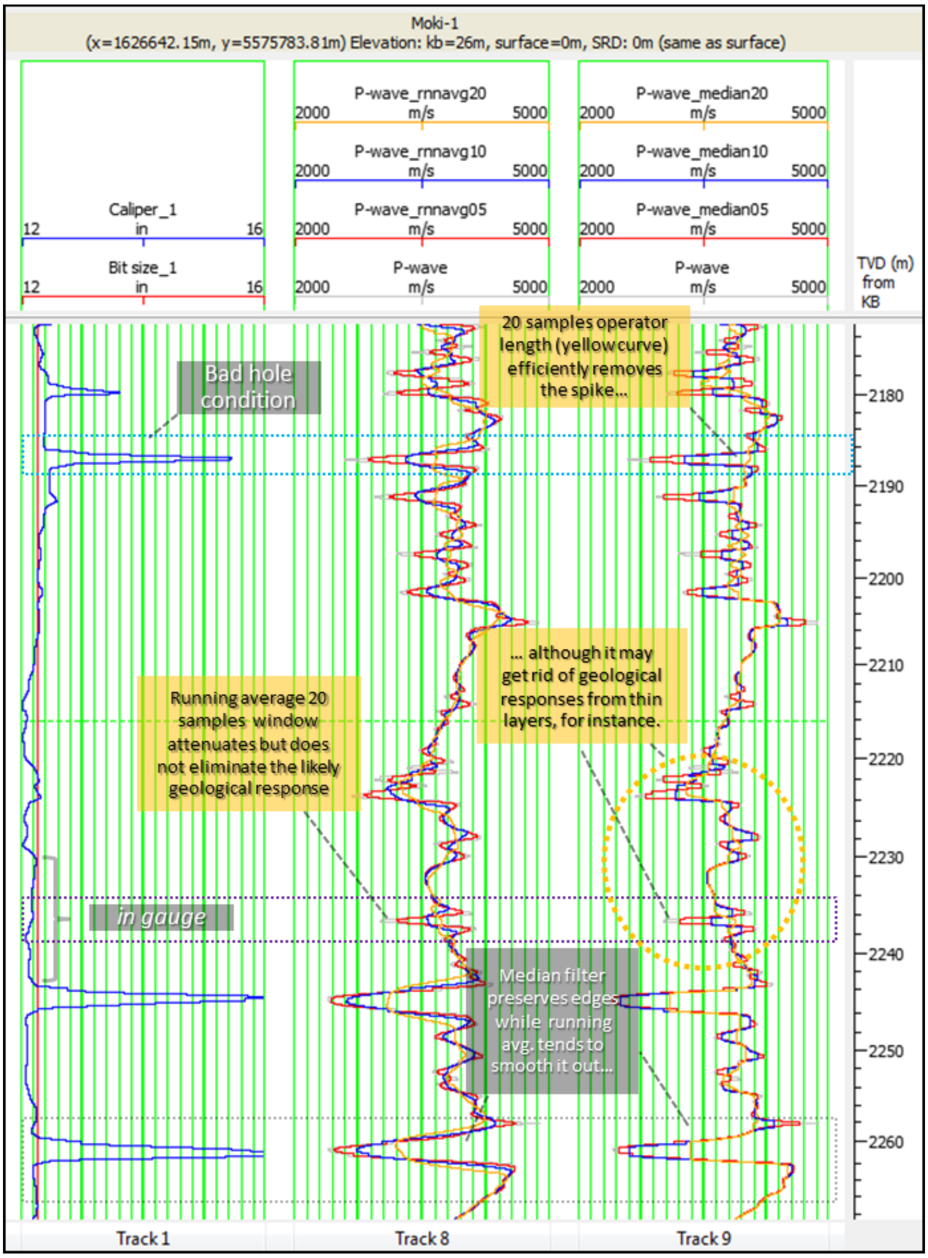

Figure 4.6: De-spiking: the effect of different window/operator lengths using running-average and median filters. The section shows an example applied to the P-wave original (gray curve) in the interval ~2174 to 2268 meters below Kelly Bushing (KB)

For the lower Manganui section alone, a trend is not reliably identifiable (Figure 4.9). The cause is likely to be due a relative low variance of the velocity and density range within this section, which makes regression incapable of explaining how these two variables vary according to one another. This is expressed by the low coefficient of determination value (r^2=0.16). An alternative approach was to estimate local parameters using the data points from the upper and lower Manganui intervals at once since they have similar lithologies. This is evident in Figure 4.8, where cross-plot (a) shows a fit for data points exclusively from upper Manganui. When lower Manganui samples are added in cross-plot (b), the same general trend is kept. Although similar lithologies occur in both zones, there is a slightly change in the fit for cross-plot (b). When we analyze upper and lower Manganui data points combined, the new parameters become $a = .303$ and $m = .257$, which is close to the original worldwide parameters established by Gardner *et al*. (1974).

Castagna *et al.* (1983) suggested using specific parameters a and m for every rock type. Even though claystone is dominant in the Upper and Lower Manganui Formations, there are still interbedded sandstones and siltstones within it. One way of separating lithologies is using Gamma-Ray (GR) as a discriminator. A GR value higher than 100 API was assumed to be claystones, while equal or less than 100 API was assumed to be sandstones or siltstones.

From the GR histogram in Figure 4.8b, it is possible to roughly infer the distribution of lithologies. A GR value of 100 API marks minus-one standard deviation from the mean value in the normal distribution curve (dashed green line), so the accumulative frequency of sandstones and siltstones (≤100 API) is around 15.9%. Using this discriminator approach, two new equations are established (Eq. 4-3 and 4-4). With density (ρ) in g/cm^3 and is P-wave velocity (V_p) in m/s, the local relationships for claystones (Figure 4.8c) and sands/siltstones (Figure 4.8d) in these two zones are, respectively:

$$\rho = 0.313 {V_p}^{0.254} \tag{4-3}$$

$$\rho = 0.301 {V_p}^{0.256} \tag{4-4}$$

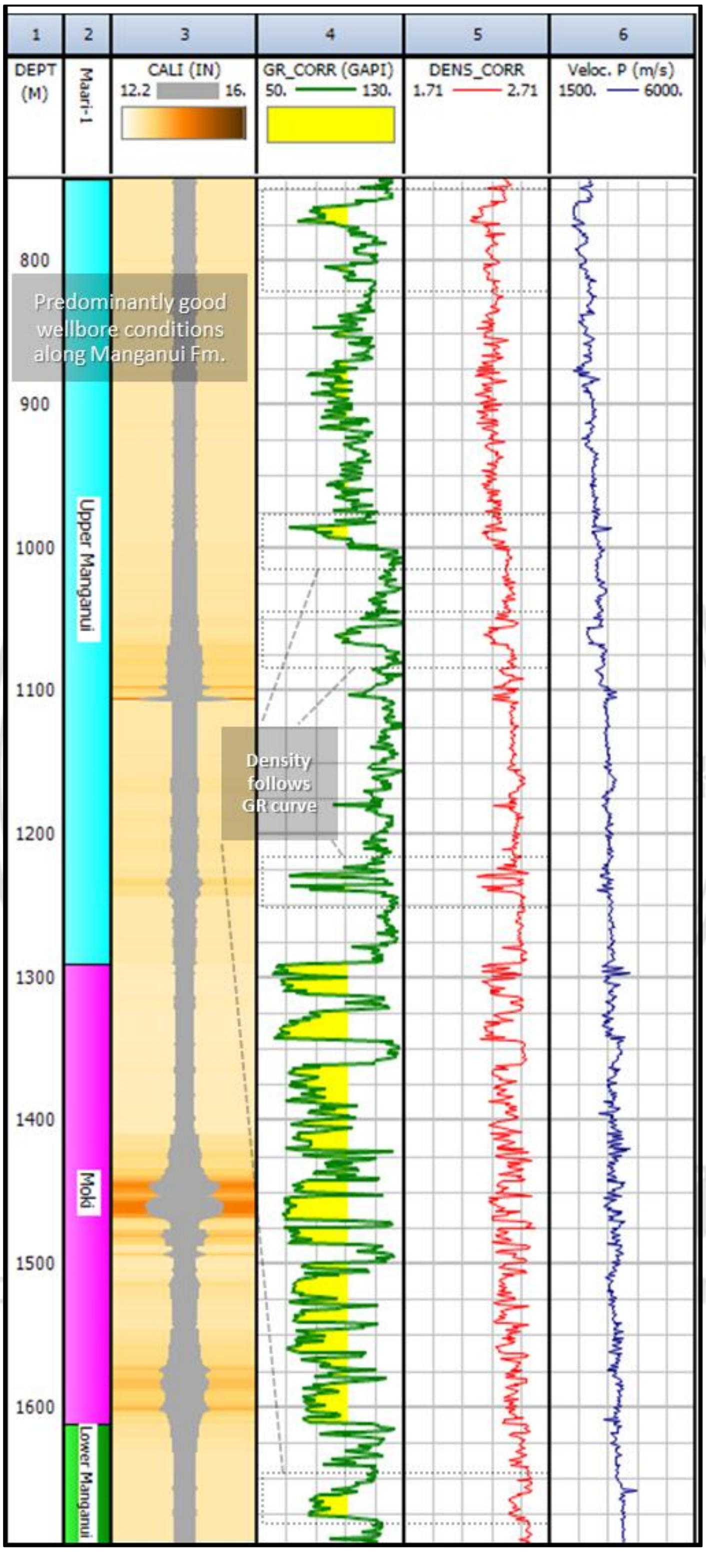

Figure 4.7: Section (~750-1700 m MD) along the well Maari-1 presenting good wellbore conditions in the Upper and Lower Manganui Fm. Consequently, a local relationship between density and P-wave velocity for these zones was based on data from this well

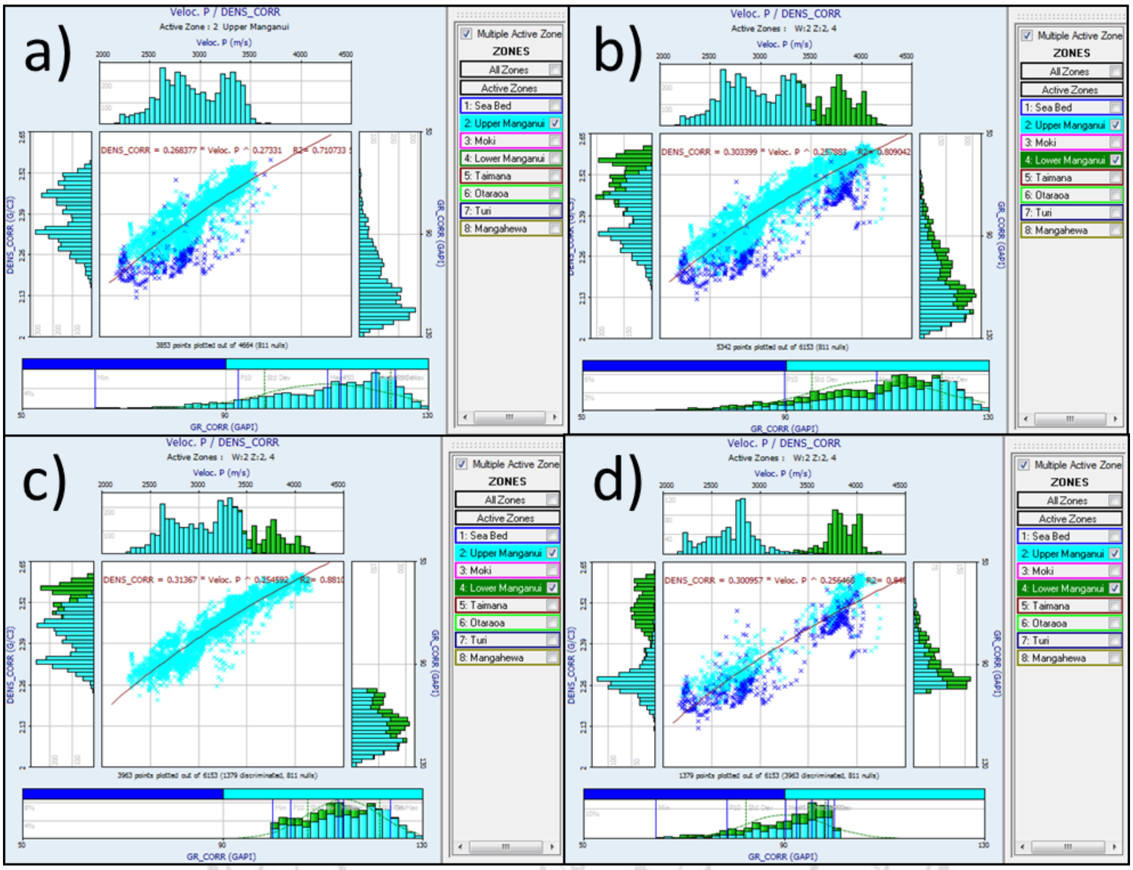

Figure 4.8: Density vs. P-wave velocity cross-plots and regression fits: (a) Upper Manganui section; (b) Upper and Lower Manganui; (c) Upper and Lower Manganui data points with a discriminator (GR >100 API) to find local Gardner's parameters for claystones; and (d) upper and lower Manganui applying a discriminator (GR ≤ 100 API) to estimate parameters for sandstone/siltstone in these formations. Note how for (b), (c) and (d) the parameters are basically the same as general Gardner's

Finally, these locally-derived parameters were applied to predict density values along the Upper and Lower Manganui Formations. Figure 4.10 presents an example from well Kea-1, which is the farthest well from Maari-1 among all available wells, comparing the original Gardner's (yellow curve) and a local relationship derived for Upper Manganui Fm. (red curve, Eq. 4-2). The interval (~1650-2200 meters) is strongly affected by wash-outs, except for a few areas where caliper is in gauge. In these zones – highlighted by red dashed rectangles – density values are reliable and might be a way to verify if the predicted log is accurate. Despite of being relatively thin intervals, the predicted log (red curve) matches quite well with the original log (black curve) and in areas in between these “control points”, the predicted log appears to follow what would be a natural compaction trend with shales (GR ≈ 130 API) at shallow section (1680 m) presenting density values of ~2.42 g/cm^3, while for a same GR value at deeper section (2185 m), densities are around 2.53 g/cm^3.

Another effective manner of evaluating a log prediction, as previously mentioned, is to perform a well-tie. The idea is quite simple, a good log prediction will result in a reasonable well-tie, i.e. reflections (frequency and amplitudes) of synthetic and actual seismic will match along the section where log is predicted. It can either be qualitatively analyzed or quantitatively (e.g. cross-correlation, etc.). Figure 4.11 illustrates the well-tie before and after log prediction in the interval along upper Manganui (shown in Figure 4.10).

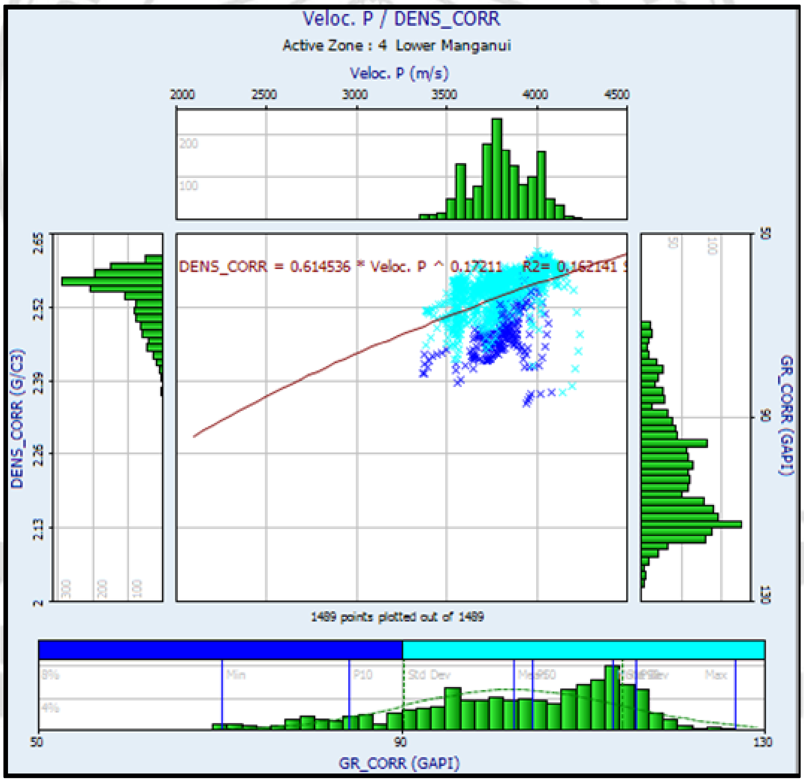

Figure 4.9: Cross-plot of density and P-wave velocity from lower Manganui zone. Power equation fit is not reliable as a low variation within the velocity range (lacking trend) seems to make it difficult to accurately relate the two variables. It is illustrated by the low correlation of determination value (r^2=0.16)

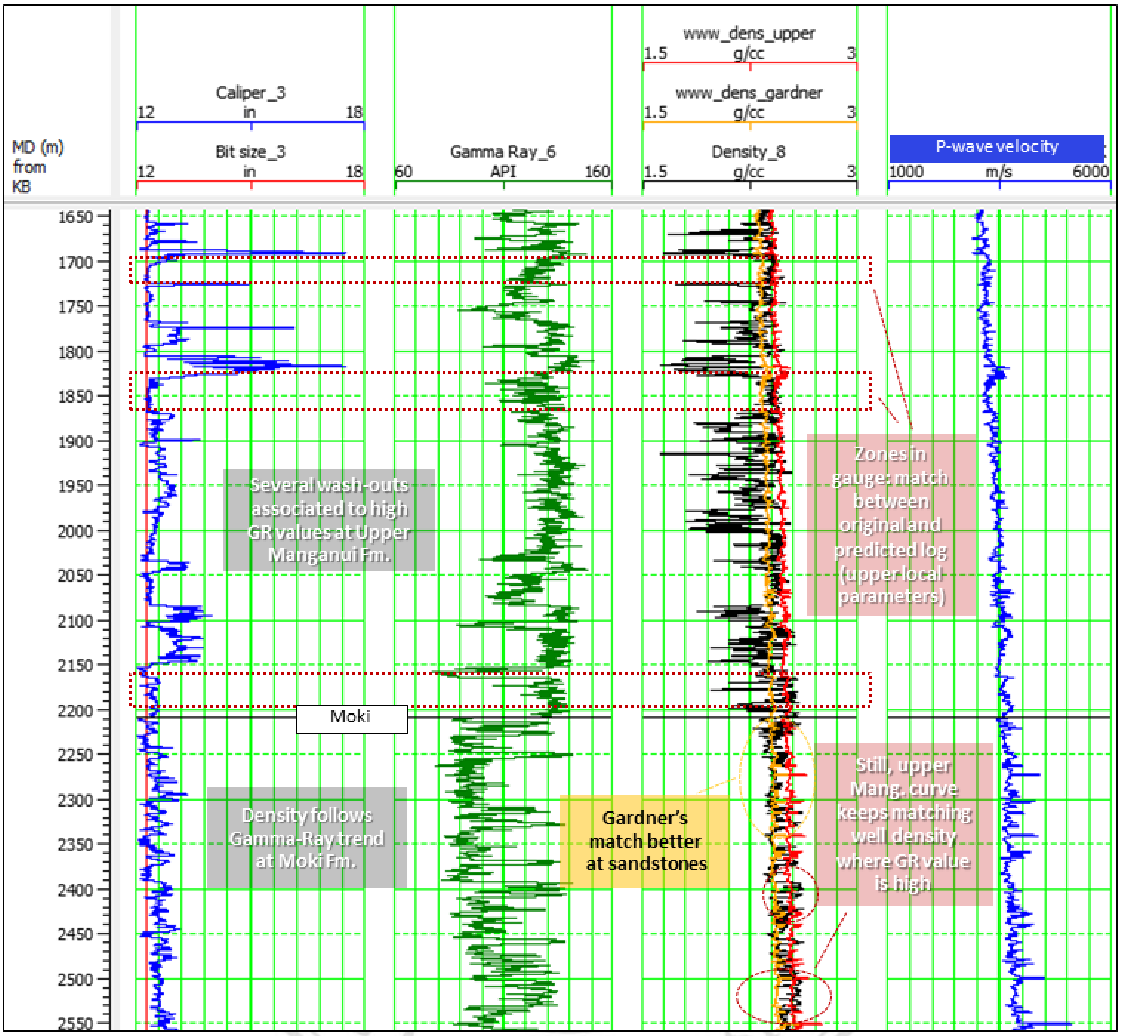

Figure 4.10: Density log prediction in an interval strongly affected by bad hole conditions in well Kea-1: comparison between original log, predicted log using local parameters for Upper Manganui Fm. (Eq. 4-2) and the general Gardner's relationship

Log prediction was also required in well Maui-4. This well was drilled in 1970 and many problems are found: (1) there is no caliper log except for a short interval of approximately 200 meters in the Turi, Mangahewa and upper part of the Farewell Fm.; (2) the sonic log is noisy, with several spikes; and (3) the density log is absent in three intervals as shown in Figure 4.13. For those reasons, a new local relationship was obtained in order to predict values in the deeper section. For the other missing sections (Upper Manganui and Lower Manganui), the local relationships previously estimated were used. The challenge in estimating a local relationship for this zone, which encompasses the Mangahewa and Farewell formations, is that most of the available wells did not reach the Farewell Fm. and the Manganui Fm. is strongly affected by wash-outs in every other well available.

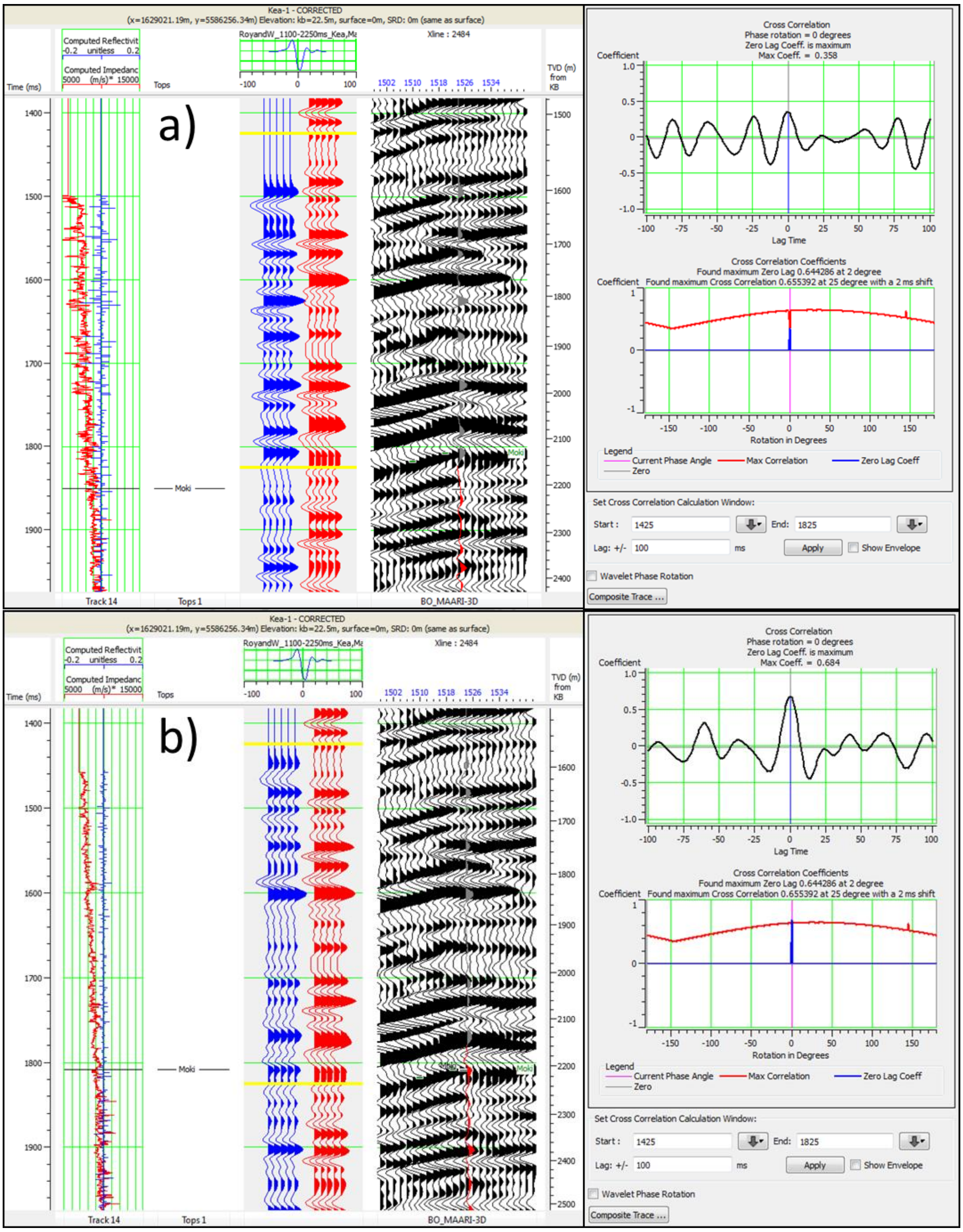

Figure 4.11: Comparison between the synthetic seismogram (blue) and actual seismic data (red) over the interval 1425-1825 ms TWTT, upper Manganui Fm. before (a) and after well log prediction (b) using Eq. 4-2 (Upper Manganui local relationship). The time-to-depth relationship is derived from the sonic log after check-shot calibration

The approach used to derive a density: Vp relationship for the deeper missing section ($\sim 2700 - 3900$ m) was to use the own original data from Maui-4. Because it is clear that bad hole conditions affected density readings (see Figure 4.13), an area had to be delimited on the cross-plot so the regression fit is applied just to the data points considered to be ‘good data’. The cross-plot presented in Figure 4.12 exhibits the data points with a frequency color scale in order to make it easier to identify the main trend. After a power fit is applied, the following relationship is established (Eq. 4-5) and used to predict density values for the section that goes from Turi marker down to the basement:

$$\rho = 0.111{V_p}^{0.372} \tag{4-5}$$

with density (ρ) in g/cm3 and is P-wave velocity (V_p) in m/s.

This relationship, along with Eq. 4-2, was used to predict density values from P-wave velocity log and results are shown in Figure 4-13. The original density log (red curve), predicted density using the upper Manganui local relationship (blue curve) and the density values obtain from applying Eq. 4-5 (black curve) are presented in Track 11. The predicted curves match relatively well their respective target zones and, particularly in the Moki Fm. and a few other intervals, the original data is acceptable, so these sections can be combined to form the final density log. In Track 9, the original P-wave velocity (black) and P-wave after de-spiking (red curve) are displayed.

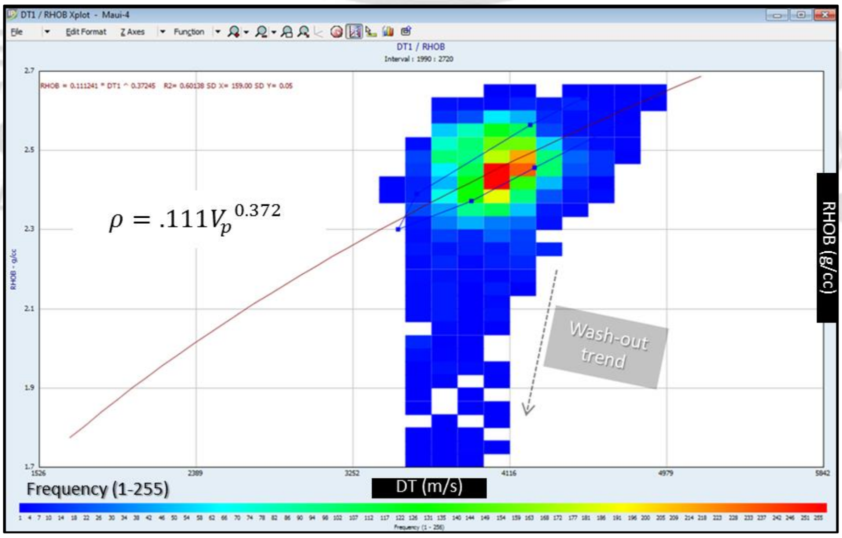

Figure 4-12: Density (g/cm^3) *vs.* P-wave velocity (m/s) cross-plot used to identify the general trend and derive a local relationship to predict missing density log in Maui-4

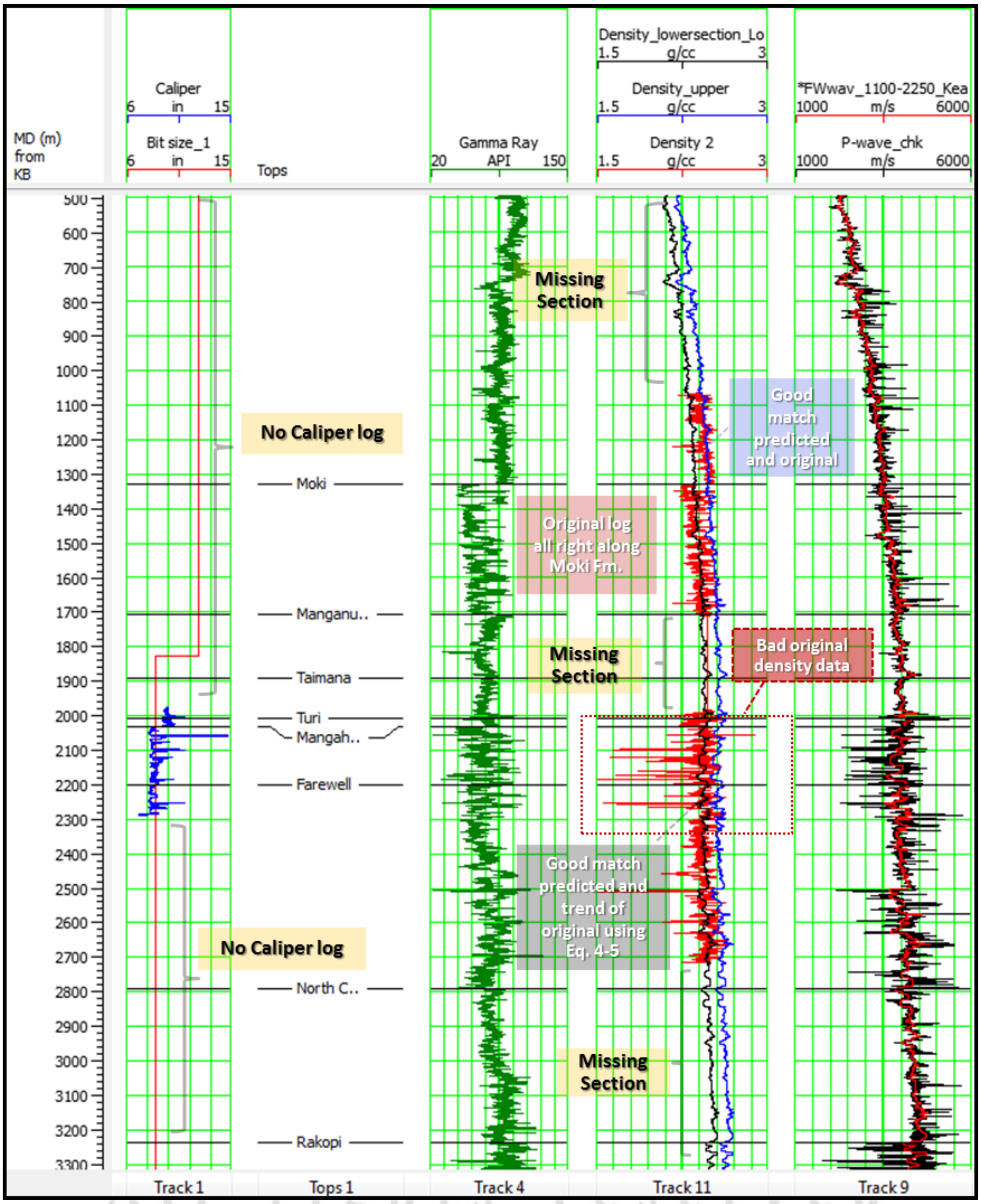

Figure 4.13: Bit size, Caliper, Gamma-Ray, original density and predicted density logs as well as P-wave velocity, original and after de-spiking, in well Maui-4. Note that there is no caliper log for most of the section. Density is also missing in long intervals. Equations 4-2 (blue curve) and 4-5 (black curve) were used to predict density from the de-spiked P-wave velocity log along these sections. The final density curve, i.e. used to create a synthetic seismogram, will be a composite of these curves (where they apply) plus parts of the original log (where in good condition)

A comparison between the synthetic seismogram and actual seismic data over the interval ~2750 – 3840 m or 1850 – 2355 ms TWTT, where there was no density log, is presented in Figure 4.14. Density values were predicted by applying Eq. 4-5 (Track 11). The P-wave velocity used to compute Impedance and reflectivity logs (Track 7) is shown in Figure 4.13 as a red curve corresponding to the original sonic after de-spiking. The match between the synthetic (red wiggle trace) and the actual seismic (black wiggle trace) is fairly decent, considering all the problems found in this well. The main reflections (top of North Cape, Rakopi and Basement) match relatively well with seismic, although the amplitudes are slightly different. Cross-correlation over the interval analyzed is 66%, which suggests an acceptable match.

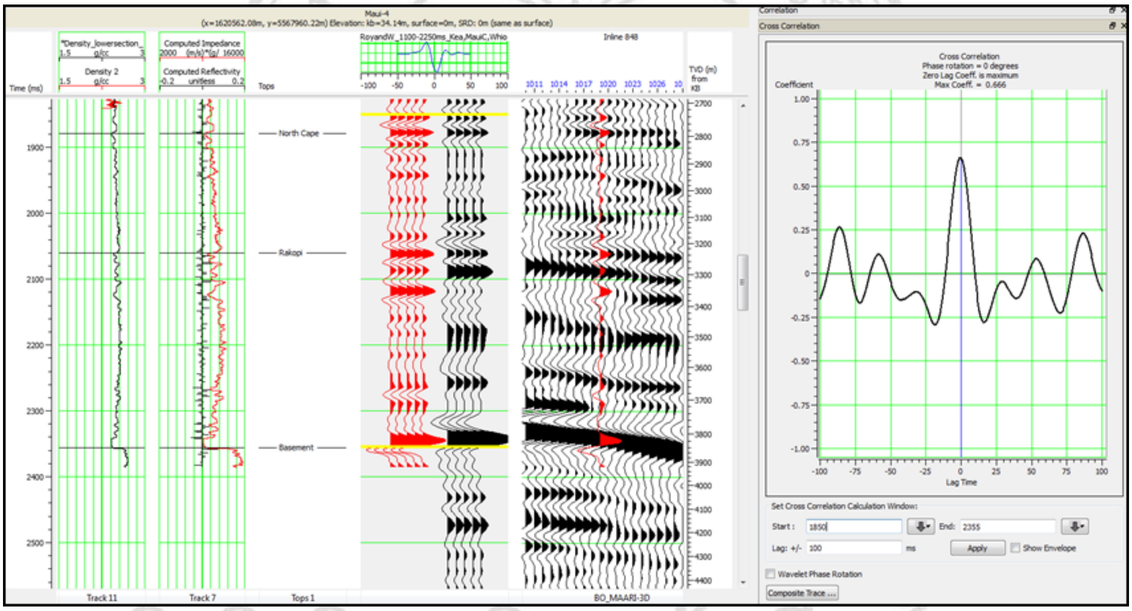

Figure 4.14: Comparison between the synthetic and actual seismic data along the interval ~2750 – 3840 m or 1850 – 2355 ms TWTT in Maui-4 after the density log was predicted from Vp using Eq. 4-5. No density log was available in the interval. The main reflection events present a fair match with the seismic data. The cross-correlation between synthetic and actual seismic trace is 66%

Ultimately, the final density and sonic curves are a collection of multiple pieces put together: predicted curves at certain intervals, zones edited by hand, de-spiked sections and, hopefully, segments of the original log. Simm and Bacon (2014) approach this question pointing to the fine line between log QC and log interpretation.

Next, the final curves along with synthetics and their matches to the seismic data (well-ties) will be individually discussed and presented. Moreover, topics that were not discussed here, such as wavelets – for instance – will also be approached in the well-ties section.

4.2 Well-Ties

Reynolds (1997) indicates that one of the main challenges associated with the seismic method is to convert the data domain from two-way travel-time to depth. It ultimately requires information about seismic velocities and for that reason great efforts are made during processing to measure this key parameter. This study though, is not intended to approach the different methods and techniques applied during seismic processing that allow conversion of seismic data from the time to depth domain. Instead, the aim here is to correlate well-log data (measure in depth) to seismic data (measured in time) through the process known as well-tying, which is essential for seismic inversion. Based on the convolutional model (Yilmaz, 1987), density and sonic (slowness) logs are used to estimate acoustic impedance and reflectivity log that are then convolved with a wavelet to create a synthetic seismogram (White and Hu, 1998). The wavelet represents the source signature and is vital in the seismic-to-well tie correlation process once it represents the link between seismic data and geology (reflectivity function). The choice of unrepresentative wavelets, i.e. wavelet containing errors in phase and frequency, is known to be one of the main reasons to poor well-ties (White, 1997).

To sum up, a synthetic seismogram simulates the seismic response at the well location, using data measured along the wellbore. Thus, a well-tie is validated in case of a reasonable match between the synthetic seismogram and the actual seismic trace. This section will briefly comment on wavelets, before presenting the final edited curves and well-ties as well as the synthetics displayed over the seismic sections.

4.2.1 Wavelet Extraction

Most of the softwares provide a whole variety of ways to use and extract wavelets. There are theoretical wavelets, such as Ricker, Ormsby, Butterworth, for example; wavelets can be extracted from seismic data, i.e. statistical wavelets; and we can estimate the actual wavelet amplitude and phase spectra by using both seismic data and well logs, known as full log extraction (see Walden and White, 1998; White and Simm, 2003; Hampson-Russell, 2015). It can be tricky though, because in order to extract a wavelet considering well log information, which would allow to estimate phase, first an optimum correlation is required.

So a common approach when tying many wells for inversion is to begin with a wavelet statistically extracted from the seismic traces through autocorrelation, in order to obtain a first correlation. During the process, a phase estimate can be inferred through an interactive window that allows testing of different phase rotations while the symmetry of the cross-correlation function can be inspected. Thus, a phase rotation can be applied to the statistical wavelet in order to re-tie with the new phase estimate. Theoretical wavelets, like the Ricker wavelet for example, can also be generated with approximated frequency content and with the estimated phase rotation in order to generate an optimal tie.

A statistical wavelet was extracted from the seismic volume over the interval 1100 to 2250 ms, which is approximately the inversion target interval, and used as a first wavelet. Due the expected polarity of seismic data, where an increase in Acoustic Impedance (AI) is a trough, before extraction the wavelet was defined to be of constant phase with a 180° phase rotation. Figure 4.15 presents this statistically extracted, constant phase, symmetric wavelet and its amplitude spectrum with a dominant frequency around 30 Hz.

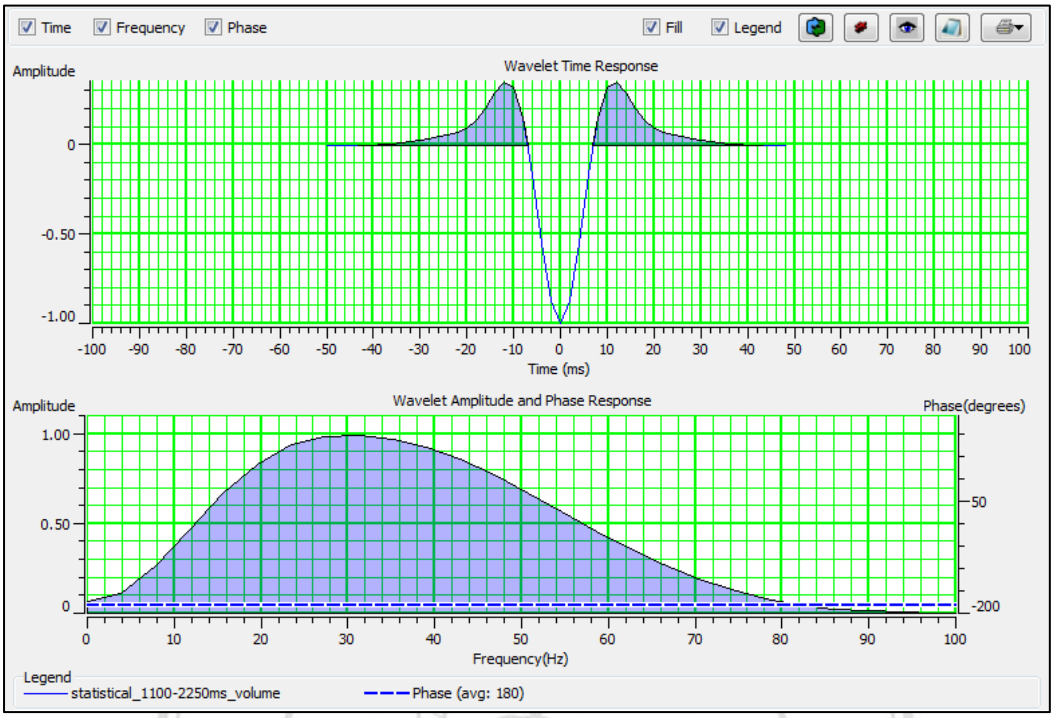

Figure 4.15: Statistical wavelet extracted over the interval 1100-2250 ms TWTT. A phase rotation of 180° was defined to match the expected polarity of the seismic data

By using this first wavelet and correlating the synthetic seismogram with the actual seismic trace, it was observed that two different wavelets with different phase rotations would be needed to tie the seven available wells. For most of the wells, it was noticed that a wavelet with a constant phase around 145° produced the best possible tie. These wells included Kea-1, Maui-4, Moki-1 and Whio-1. The wells Maari-1 and Maari-2, on the other hand, had an optimal correlation with a nearly 90° phase wavelet. Figure 4.16 illustrates the procedure just described. Then, Ricker wavelets with a central frequency of 30 Hz and 145° and 90° phase were created to tie the wells (Figure 4.17). After the best possible correlations were obtained with these wavelets, a full log extraction was used to estimate wavelet properties at each well (amplitude and phase spectra). If our phase assumptions thus far were reasonable, the phase of the full waveform extracted wavelets should not differ much from the phase approximations made by using the theoretical Ricker wavelets. Figure 4.18 presents the extracted wavelets from each of the wells. They can be divided in two groups with base on the estimate phase: a) including Kea-1, Maui-4, Moki-1 and Whio-1; and b) including Maari-1 and Maari-2.

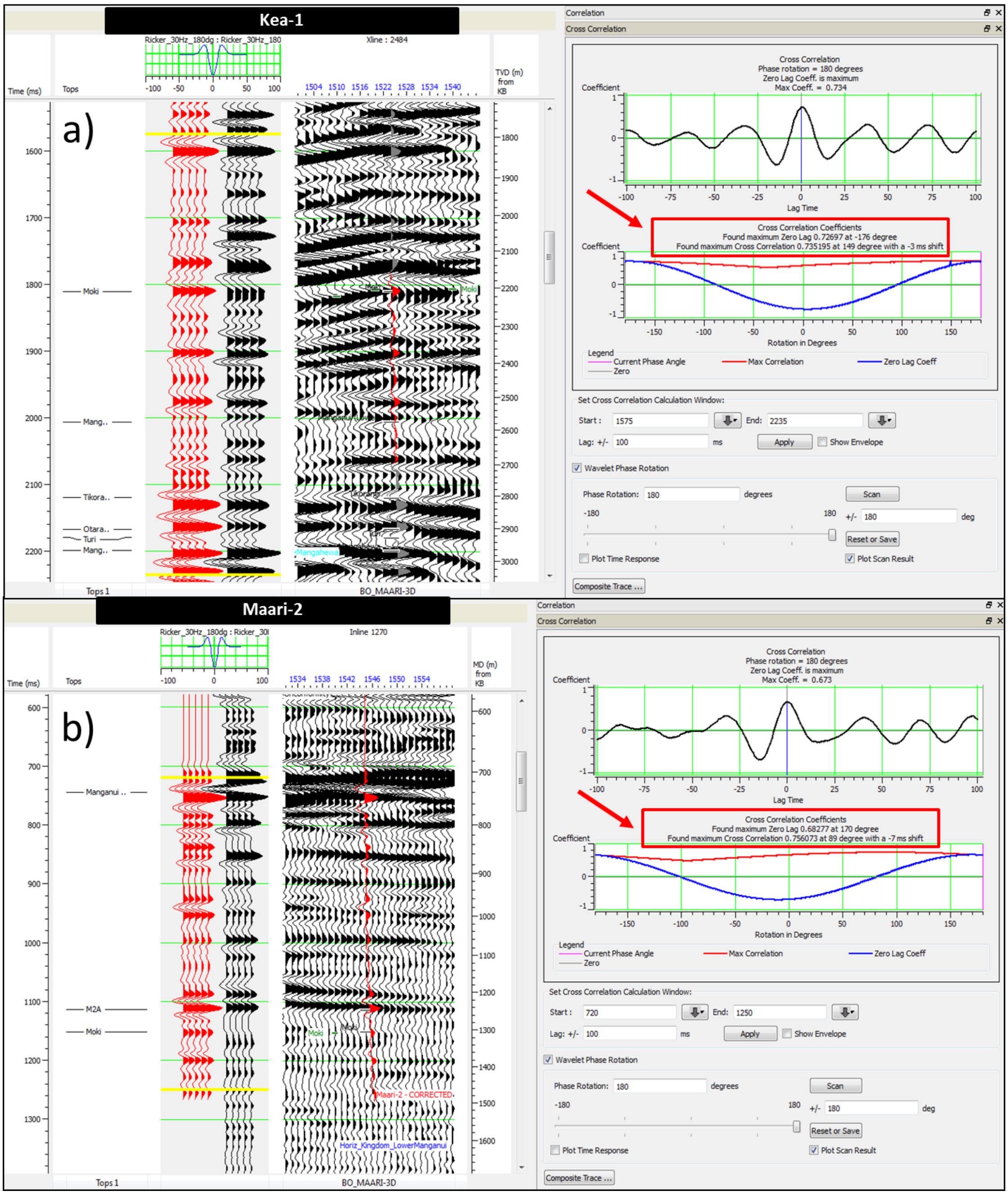

Figure 4.16: Initial statistical wavelet used to obtain a preliminary tie. During the process, information about phase can be estimated. Note how the cross-correlation function in (a) and (b) are asymmetrical. Phase to reach maximum cross-correlation is indicated (red rectangle) for wells Kea-1 and Maari-2 (149° and 89°, respectively)

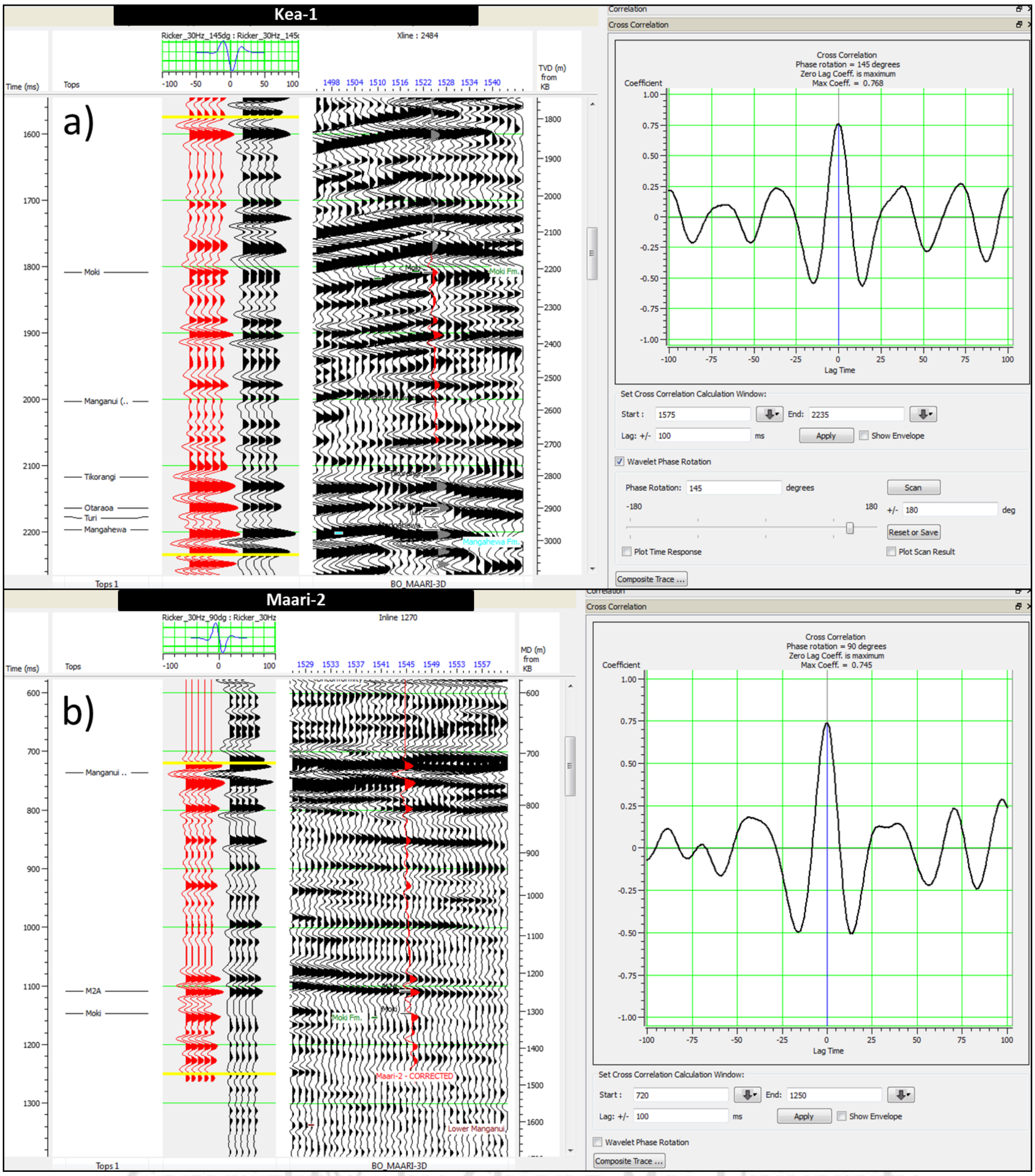

Figure 4.17: Seismic-to-well-tie with a 30 Hz Ricker wavelet. Phase rotation is at Kea-1 (a) 145° and at Maari-2 (b) 90°, as suggested in Figure 4.16. Note how the cross-correlation function in (a) and (b) are nearly symmetrical after the phase rotation

To extract the final wavelet, only the wells Kea-1, Maui-4, Whio-1 and Moki-1 (see Figure 4.18) were considered. The choice of these wells is justified by the fact that they share approximately the same phase. Figure 4.19 presents the extracted average wavelet in time and frequency domain, i.e. its amplitude and phase spectra. The extraction used a full log approach (Roy and White Method) over the target interval

1100-2250 ms. This wavelet, from now on, will be referred to as the final wavelet, as it represents a representative average wavelet from the well ties.

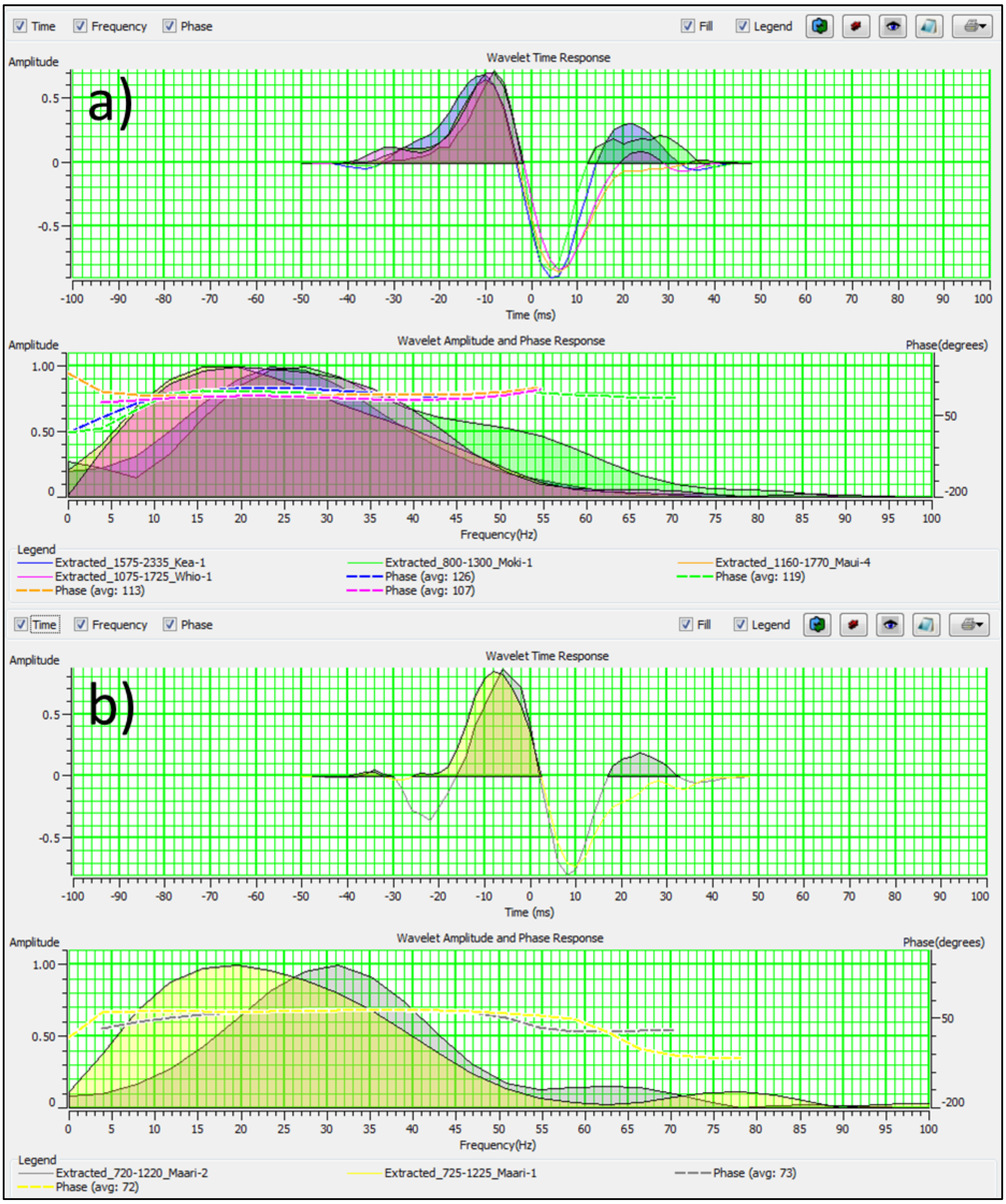

Figure 4.18: Extracted wavelet from each well using a full log approach. With base on the phase estimate, they are divided into two groups of wavelets: a) including Kea-1, Maui-4, Moki-1 and Whio-1; and b) including Maari-1 and Maari-2. The phase estimates is considered to be within an acceptable variation range from the previously thought 145° phase group (a) and the 90° phase group (b)

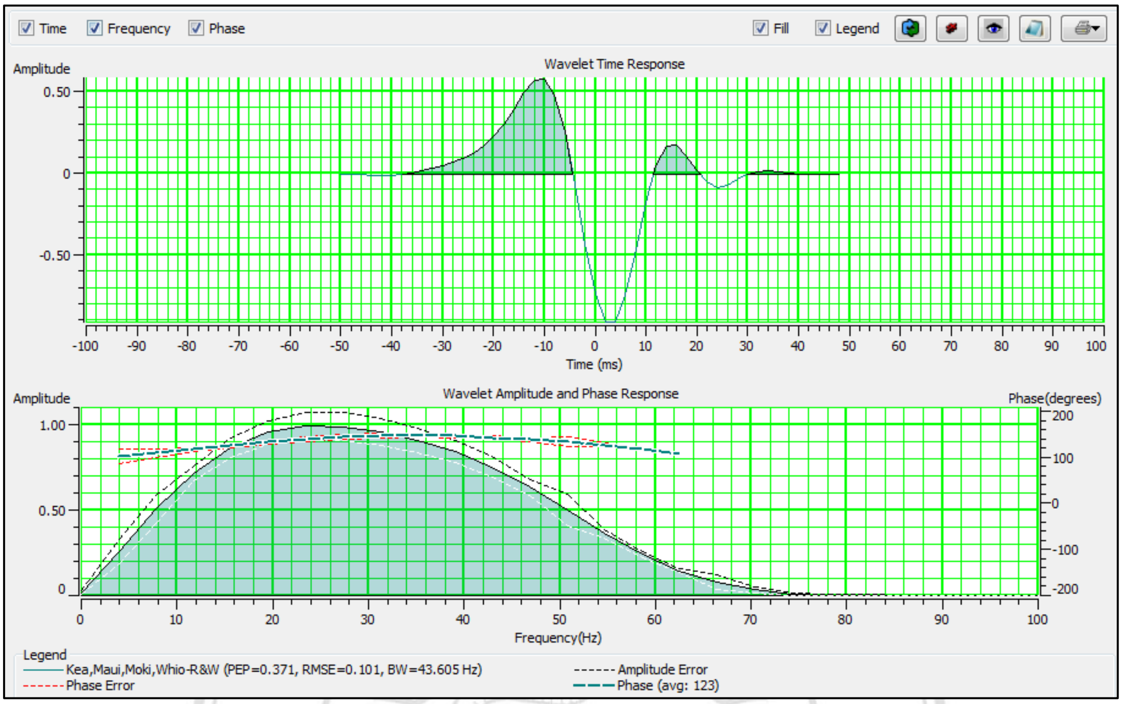

Figure 4.19: Final average wavelet extracted using wells Kea-1, Maui-4, Moki-1 and Whio-1 by a full log approach over the interval 1100-2250 ms. Wavelet is shown in time and frequency domain (amplitude and frequency spectra). Average phase is 123° and dominant frequency around 26 Hz

It is also worth mentioning about the choice of windows (zones, intervals) where the cross-correlation was measured at each well during the seismic-to-well tie process. In this study, due to a couple of factors, these zones vary significantly. There is the own natural complexity associated with the geology, like dipping layers, fault block movements, etc., as well as circumstances inherent to the well-log data and the seismic method that might influence the position and length of these zones along the well path. As a primary target, the top of Moki Fm. varies in the time domain from approximately 1100 to 1800 ms TWTT. The ideal would be to get good ties around the target, with some significant seismic events above and below presenting a good match with the synthetic seismogram adding some confidence to the process. Commonly, a window of at least 500 ms is required to make the cross-correlation function reliable. Sometimes, limitations regarding the depth reached by the wells also affect this choice. Maari-2, for instance, was drilled to a total depth of 1494.90 meters, which is still inside the sandstones of the Moki Fm. The well Maui-4 was the only well that penetrated the whole stratigraphic column in the study area.

Seismic data quality also influences the place of these windows, due to zones where amplitudes were not preserved or because there a lack of significant seismic events to be correlated, for example, forcing the window to be shifted up or down. As mentioned in Section 1.2, the 3D Maari seismic data presents several zones where amplitudes were partially attenuated by a highly reflective overburden and local shallow gas anomalies. It happens around many well locations as it will be shown next. The well Moki-2A is an extreme case, where the amplitudes were so strongly attenuated that it was not possible to tie seismic and well data.

Table 4.2 summarizes the impact of wavelets on well-tie quality by showing the change of cross-correlation coefficient for different wavelets at each well. The "full extraction" refers to the local extracted wavelet presented in Figure 4.18 and the "final wavelet" refers to the wavelet presented in Figure 4.19, extracted by the Roy-White Algorithm (Hampson-Russell, 2015) using Kea-1, Maui-4, Moki-1 and Whio-1.

Table 4.2 – Relation of wavelet and respective cross-correlation coefficient obtained over the respective intervals for each of the wells investigated.

Well Name	Wavelet	Cross-correlation	Interval
Kea-1	Statistical (180° phase)	.72	1575 - 2335 ms
	30 Hz Ricker (145° phase)	.74	
	Full Extraction (126° phase)	.78	
	Final Wavelet	.81	
Maari-1	Statistical (180° phase)	.68	725 – 1225 ms
	30 Hz Ricker (90° phase)	.74	
	Full Extraction (72° phase)	.79	
	Final Wavelet	.73	
Maari-2	Statistical (180° phase)	.67	720 – 1220 ms
	30 Hz Ricker (90° phase)	.76	
	Full Extraction (73° phase)	.77	
	Final Wavelet	.71	

Table 4.2 (Continued)

Well Name	Wavelet	Cross-correlation	Interval
Maui-4	Statistical (180° phase)	.62	1160 - 1770 ms
	30 Hz Ricker (145° phase)	.63	
	Full Extraction (113° phase)	.68	
	Final Wavelet	.66	
Moki-1	Statistical (180° phase)	.68	800 – 1300 ms
	30 Hz Ricker (145° phase)	.69	
	Full Extraction (119° phase)	.74	
	Final Wavelet	.74	
Whio-1	Statistical (180° phase)	.72	1075 – 1725 ms
	30 Hz Ricker (145° phase)	.74	
	Full Extraction (107° phase)	.78	
	Final Wavelet	.77	

4.2.2 Kea-1

Seismic traces along the well path of Kea-1 present a lot of significant events that make it easier to correlate with the synthetic. The top of Tikorangi, a limestone, marked by a high-amplitude trough (i.e. an increase in acoustic impedance, soft to hard rock) around 2120 ms (TWTT) and also the high amplitude peak characterizing the top of Mangahewa Fm., a secondary reservoir target around 2200 ms (TWTT), are good examples. The analyzed cross-correlation window had over 750 ms length (1575-2235 ms TWTT) and exhibited a good correlation due the fact the seismic data seems to present a fairly good signal-to-noise ratio at this part of the Maari 3D area. Unfortunately, it does not happen in other regions where there imaging issues due to bad acquisition, gas anomalies causing attenuation of amplitudes, etc.

The seismic to well-tie for Kea-1 is presented in Figure 4.20 along with the main curves (Gamma-Ray, Density, P-wave velocity, Computed Impedance and reflectivity) before (original log) and after log editing. The final density and P-wave velocity curves are indicated by an asterisk (red and blue curve in Tracks 3 and 5, respectively). Figure

4.27 displays the colored computed synthetic seismogram over the seismic section (IL 1524).

4.2.3 Maari-1

The analyzed time window in Maari-1 was restricted to the interval 725-1225 ms (TWTT), including the upper Manganui and a part of the Moki Fm., where there are seismic events to correlate. Below that, a reflection-free zone occurs and is clearly observable in the computed reflectivity log in Track 7. Even the sharp reflection at top of Mangahewa (peak, i.e. decrease in AI – hard to soft rock) seems to be absent in the seismic data (Figure 4.28). The colored synthetic trace displayed over the seismic data show that amplitudes match quite well in the upper section (above Moki) and below that there is a zone where amplitudes seem to have been attenuated in the seismic data (black ellipse). Below the Lower Manganui horizon, the lack of amplitudes probably has a geological cause since a reflection free-zone follows the horizons delimiting the formation.

The well data at Maari-1 does not seem to be much affected by bad hole conditions, despite the caliper indicating that the entire section is slightly washed-out and a few more severe washed-out zones are seen, particularly at Moki and Mangahewa formations (Figure 4.21). Consequently, the original logs were used, after eliminating some spikes, to compute Impedance and reflectivity logs. Log prediction was only used to substitute original data at the Mangahewa Fm. using the general Gardner's relation, which presented a good match for reservoir sections in Maari area (see Figure 4.10). A 73% cross-correlation in the analyzed window indicates a fairly good match between the synthetic seismogram and the actual seismic trace, even with the known phase difference illustrated by the asymmetric cross-correlation function which is caused by the final wavelet (avg. phase 123°) being different from wells Maari-1 and Maari-2, whose phase is estimated to be around 90° degrees (see Figures 4.16b) and 4.17b). It could be an indicative of how the wavelet vary with depth/time due to attenuation effects, but the Moki-1 well used a similar window (800-1300 ms) and estimated wavelet indicates phase around 145°.

3.2.4 Maari-2

The cross-correlation window at Maari-2 included basically all the well data available. The interval is delimited by the fact the well was drilled to a bottom depth of approximately 1494 m below KB. Yet, the interval is similar to the one analyzed in Maari-1. These are crestal wells just 1.25 kilometers apart. Cross-correlation between calculated synthetic seismogram and actual seismic trace in Maari-2 is 71%, showing a good match in shape and amplitude with the main seismic events – particularly top of upper Manganui Fm. (trough, i.e. increase in AI) and top of M2A sandstones (peak, i.e. hard to soft kick). Figure 4.29 shows the colored synthetic trace over seismic Xline 1545. Note how amplitudes vary laterally (highly discontinuous horizons). A possible shallow gas anomaly attenuates amplitudes in the eastern side of Maari-2 (black ellipse). By looking at the synthetic trace displayed over a seismic section, even zones where amplitudes are attenuated along the well path can still be visually correlated in order to make sure it is a reasonable tie. In this context, results for Maari-2 well are considered acceptable.

The wireline logs from Maari-2 did not require much editing or predictions to fill missing sections. Only spikes were attenuated from density and sonic logs as they did not seem to be a response from the geological medium, a hypothesis that was then supported by an increase in the correlation after the de-spiking process. Figure 4.22 presents the main curves, original and final curves used to create the synthetic trace. The presented cross-correlation function is asymmetric for the same reason as explained for the well Maari-1.

3.2.5 Maui-4

The well Maui-4 is the only well that penetrates the entire stratigraphic column in the Maari 3D seismic area, reaching a bottom depth of 3926 m below KB. The well was drilled in 1970 and presents many problems that have been discussed earlier at the log prediction section. The density log, in particular, with its missing sections and zones where bad hole conditions are the most likely cause of poor data quality (there is no caliper log), offered challenges during log editing. Many tests were performed and the end result is the only just-acceptable well-tie presented in Figure 4.23.

The colored synthetic trace computed during the seismic-to-well tie process is displayed over an arbitrary line in Figure 4.30. Note how the high-amplitude seismic reflections in the seismic data present a fairly good match with the synthetic, not just in the analyzed window, but pretty much along the entire section. Despite that, the cross-correlation coefficient indicates only a moderate well-tie quality (67%).

3.2.6 Moki-1

The analyzed window in Moki-1 well goes from 800-1300 ms, where there are several seismic events to correlate. Well data quality in Moki-1 does not seem to be compromised despite the fact that the caliper log indicates most of the section is washed-out. Thus, the final density log comes in large part from the original curve and in a few locations from a density curve obtained in the Emerge module available in CGG Geoview HRS software (Hampson-Russel, 2015). It used a multilinear regression to predict density values for Moki-1 based on Gamma-Ray and Sonic logs from all other wells. Emerge predicted density values were used on spurious zones along the Mohakatino (Upper Manganui), Lower Manganui, Otaraoa and Mangahewa formations. All the main curves from Moki-1 as well as the synthetic seismogram and the cross-correlation function are presented in Figure 4.24.

The colored synthetic trace computed during the well-tie procedure in Moki-1 is displayed over the seismic section (XL 1645) in Figure 4.31. High-amplitude events seen in the synthetic seismogram below the Lower Manganui horizon are not seen in the seismic data. In the analyzed window though, events in the seismic data and synthetic seismogram present a decent match, not just in waveform but also in amplitudes, which is indicated by a correlation coefficient of 74%.

3.2.7 Whio-1

The cross-correlation window in the deviated well Whio-1 included most of the well data available, from approximately 1075-1725ms TWTT or 1400-2600 m MD below KB. Cross-correlation between the synthetic seismogram and actual seismic trace in Whio-1 is 77%, showing a good match (Figure 4.25), especially at the zone containing a few high-energy seismic reflections below the Turi Fm. (~2330m MD). Above that, there are just a few distinguishable reflections on seismic and their amplitudes normally present significant lateral variations. One example is the reflection immediately above the M2A sand unit, around 1090 ms TWTT (Figure 4.25). These lateral variations are observed quite often in the Maari 3D seismic volume, which can be caused due geology, but also could be provoked during processing. It makes interpretation quite difficult and, as mentioned earlier, might have implications on future inversion results. Figure 4.32 presents the colored synthetic trace over the seismic section (IL 1438).

The well data at Whio-1 was affected in some intervals by bad hole conditions, with the most severe case occurring at the Mangahewa Fm., where sonic measurements as well as density measurements were unrealistic. Local relations obtained to predict density from the P-wave velocity log were applied to substitute spurious data in these zones. The general Gardner's relationship was used to predict data along a wash-out zone in Moki Fm (lower), as it was seen in other wells to be a good approximation for sandstones in the Maari area. Spikes in the sonic log were attenuated by applying a median filter. In the zone where the logs seem to have been affected by bad hole conditions (below 1600 ms TWTT), a larger window operator had to be used as sharp spikes remained and were degrading the well-tie at that zone. After that, the cross-correlation improved, resulting in quite a decent match overall. The final curves used to compute Impedance and reflectivity logs are marked with an asterisk in Figure 4.25, which presents the other main curves as well as the well-tie for the Whio-1 well.

3.2.8 Moki-2A

The Moki-2A well could not be tied to the seismic data because it is located in a zone where amplitudes were completely attenuated. Thus, the synthetic trace cannot be compared to actual seismic traces, as showed by Figure 4.26, where the track BO_MAARI-3D exhibits not a single correlatable reflection below the Upper Manganui marker. It is even clearer when the well is displayed over the seismic section, Xline 1455. Figure 4.33 shows Moki-2A located in this zone where amplitudes were highly attenuated, possibly by some shallow gas event absorbing most of the energy. A slight push-down (?) (yellow dashed ellipse, Figure 4.33) is associated with the last strong reflections (around 375 ms TWTT). Below that, the amplitudes have vanished, which makes a well-tie impossible.

The density curve from the Moki-2A well seemed to be affected by bad hole conditions in the Upper Manganui Fm., so the local relationship (Eq. 4-2) was applied and the values used in these areas. A few spikes were manually removed. The sonic log just went through the de-spike process to attenuate its spikes.

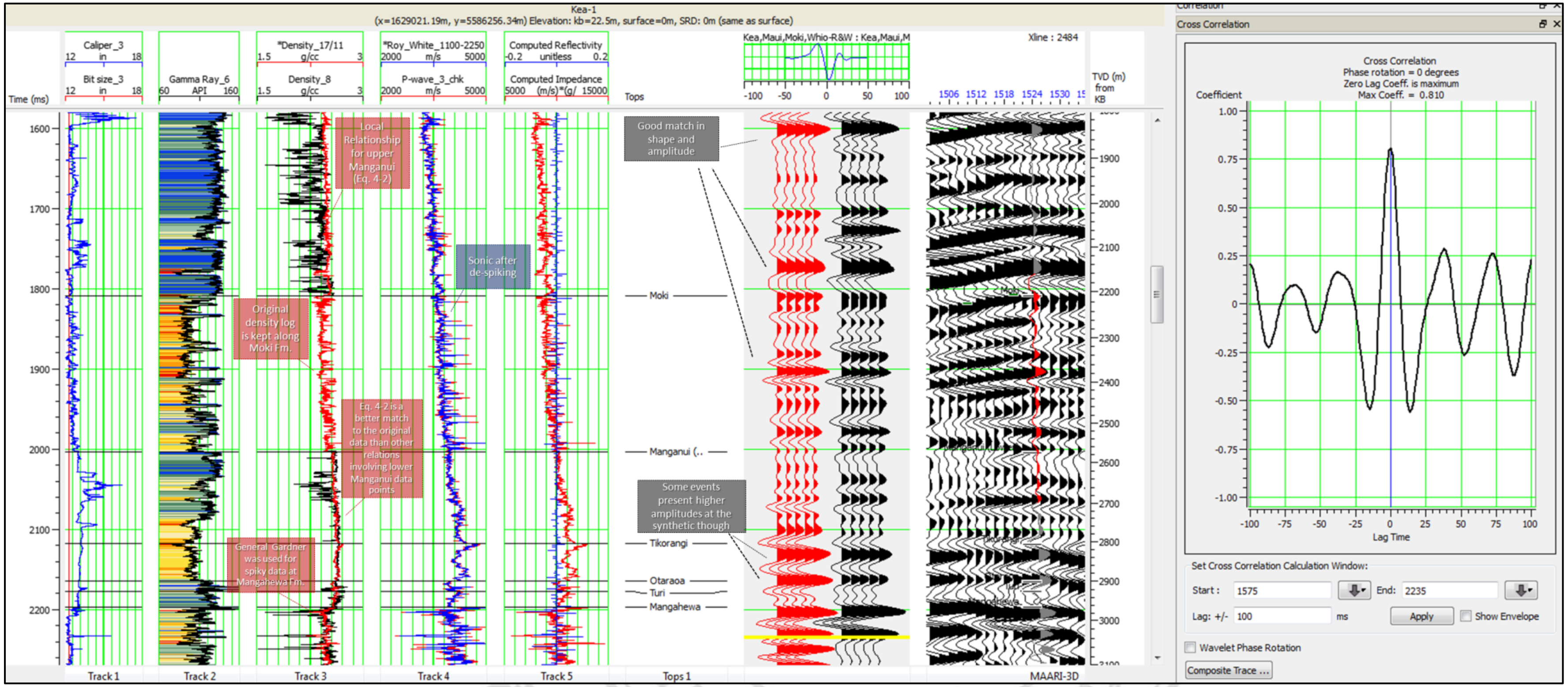

Fig 4.20: Seismic-to-well-tie in Kea-1. Original and final logs are presented. Final logs used to compute Impedance and reflectivity logs are indicated by an asterisk (*). The final density is a composite of many different segments joined together. The sonic log went through a de-spiking process and then was converted to P-wave velocity (m/s). The final wavelet (Figure 2-19) is convolved with the computed reflectivity log (Track 6) to generate the synthetic seismogram (red traces). Synthetic and actual seismic traces exhibit good correlation (81%) over the window 1575-2235 ms TWTT

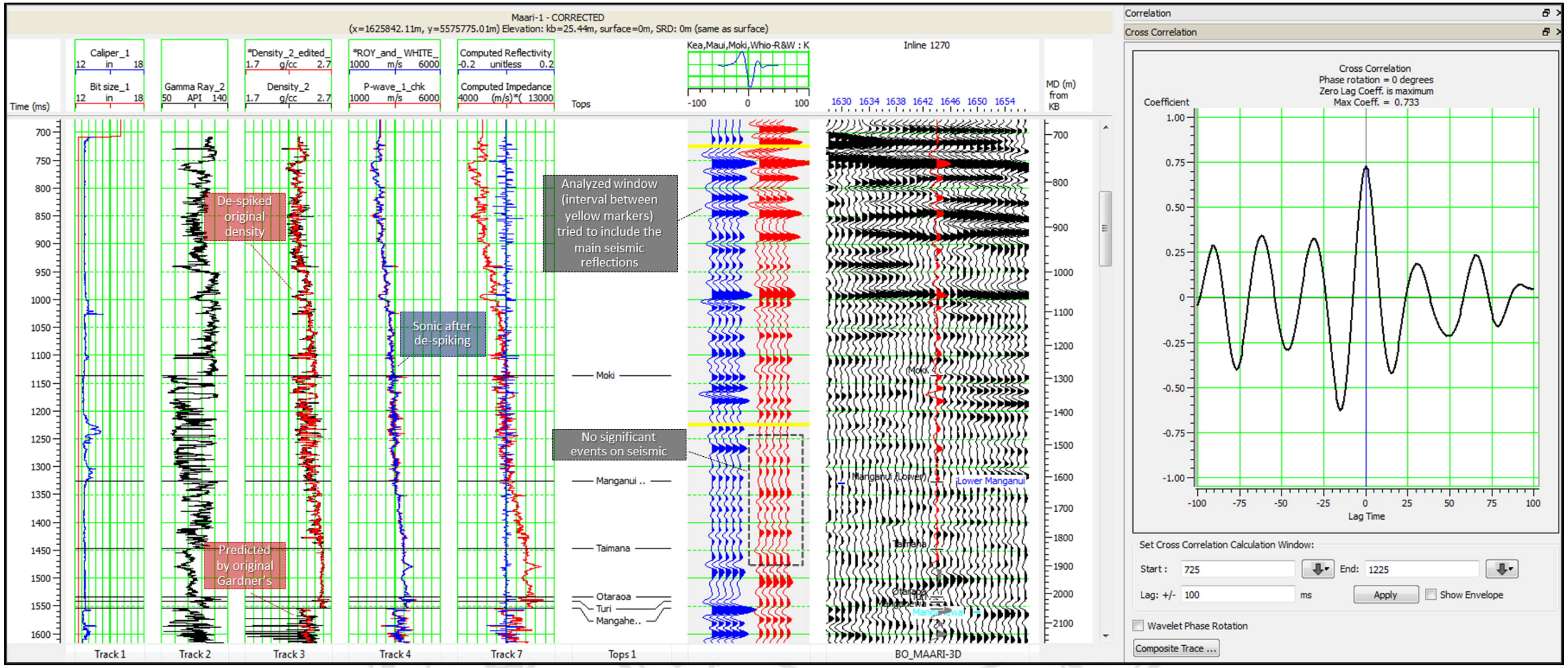

Figure 4.21: Seismic to well-tie in Maari-1. Original and finals logs are presented. Final logs used to compute Impedance and reflectivity logs are indicated by an asterisk (*). Synthetic and actual seismic trace exhibit a fairly good correlation (73%) over the window 725-1225 ms TWTT

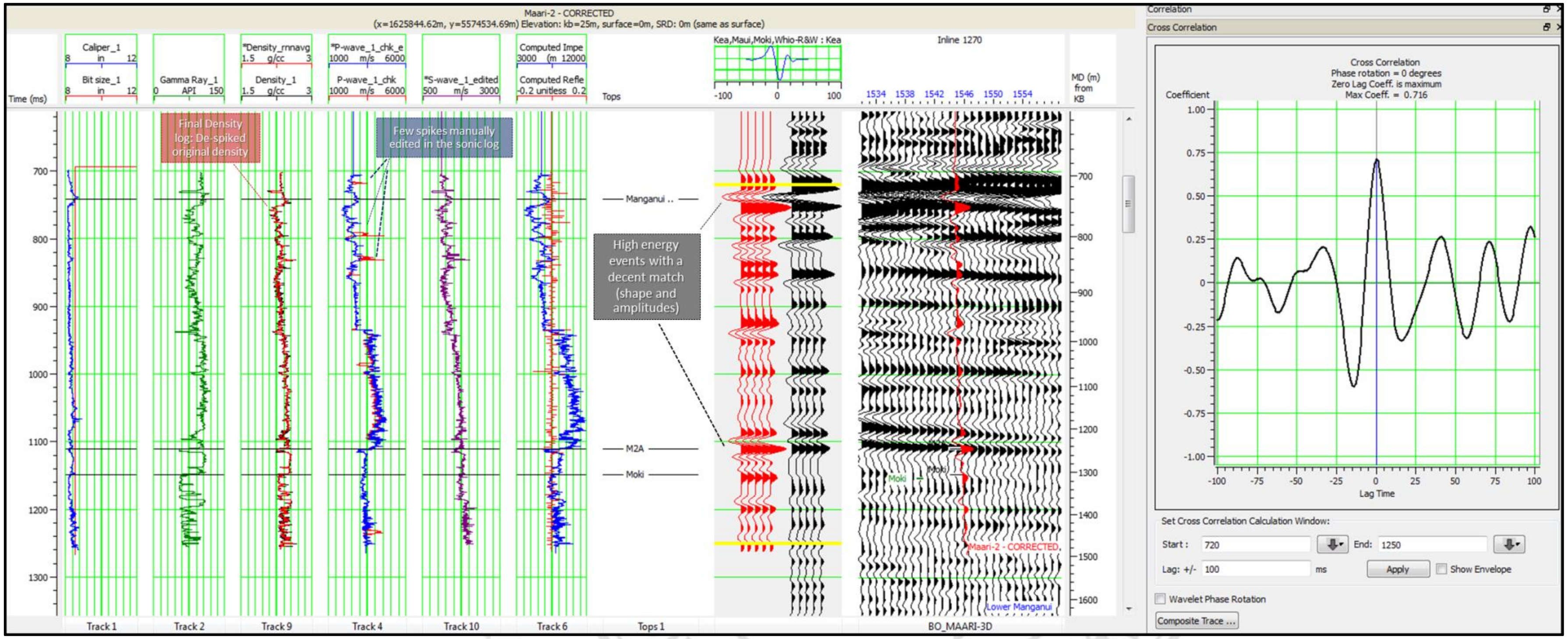

Figure 4.22: Seismic-to-well-tie in Maari-2. Original and final logs are presented. The final density (red curve, Track 9) and P-wave velocity (blue curve, Track 4) logs used to compute Impedance and reflectivity logs are assigned with an asterisk (*). Synthetic and actual seismic traces exhibit a reasonable cross-correlation (71%) over the window 720-1250 ms TWTT

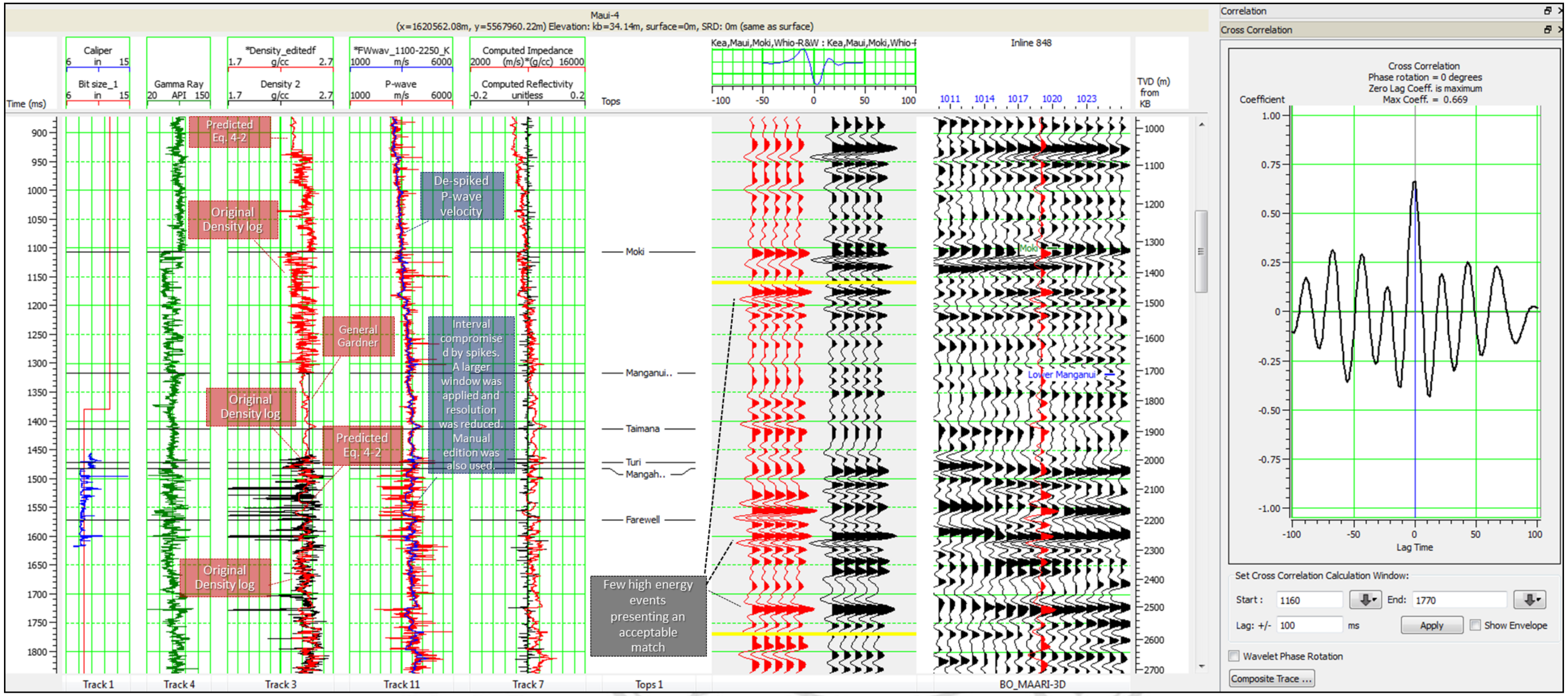

Figure 4.23: Seismic-to-well-tie in Maui-4. Original and finals logs are presented. The final density (red curve, Track 3) and P-wave velocity (blue curve, Track 11) logs used to compute Impedance and reflectivity logs are assigned with an asterisk (*). Synthetic and actual seismic trace exhibit an acceptable cross-correlation (67%) over the window 1160-1770 ms TWTT

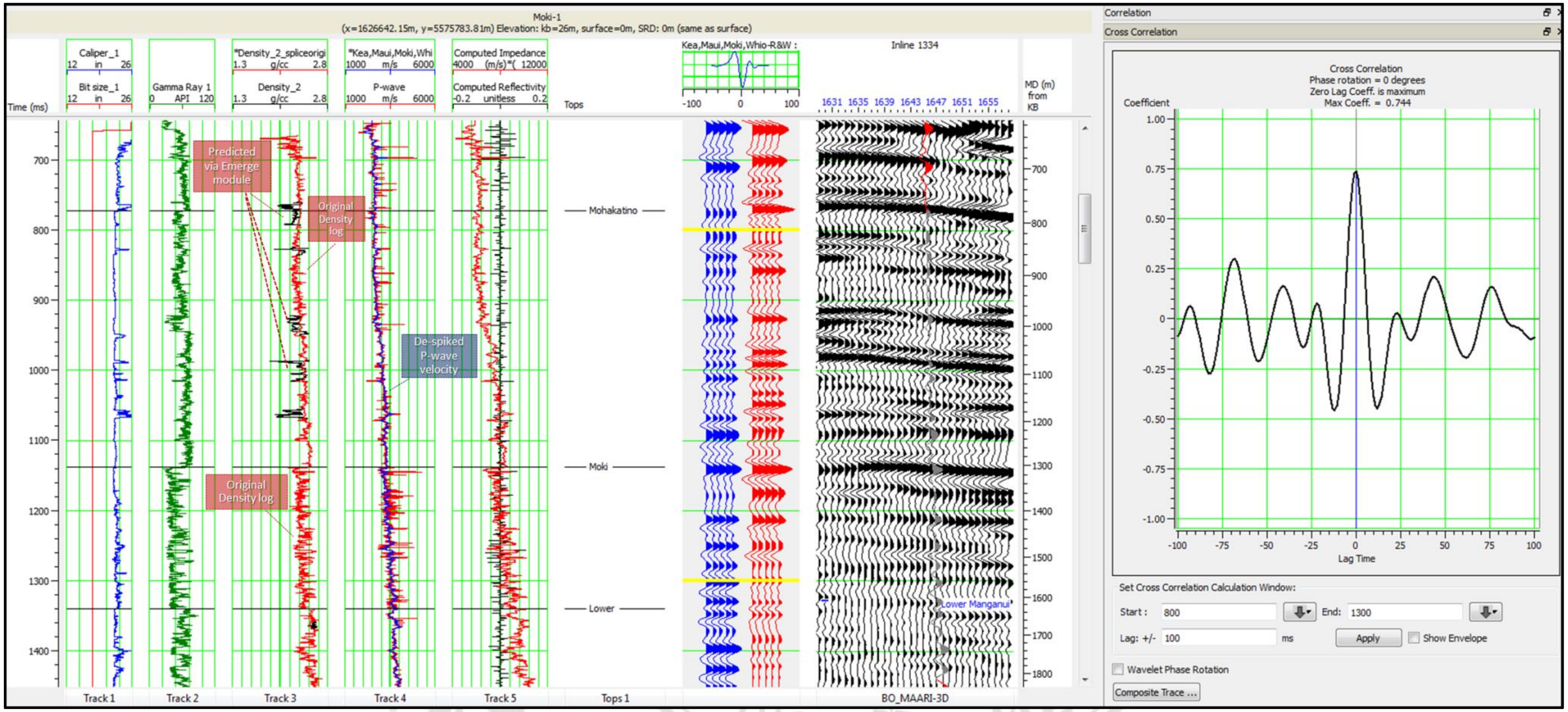

Figure 4.24: Seismic-to-well-tie in Moki-1. Original and finals logs are presented. The final density (red curve, Track 3) and P-wave velocity (blue curve, Track 4) logs used to compute Impedance and reflectivity logs are assigned with an asterisk (*). Synthetic and actual seismic trace exhibit a good cross-correlation (74%) over the window 800-1300 ms TWTT

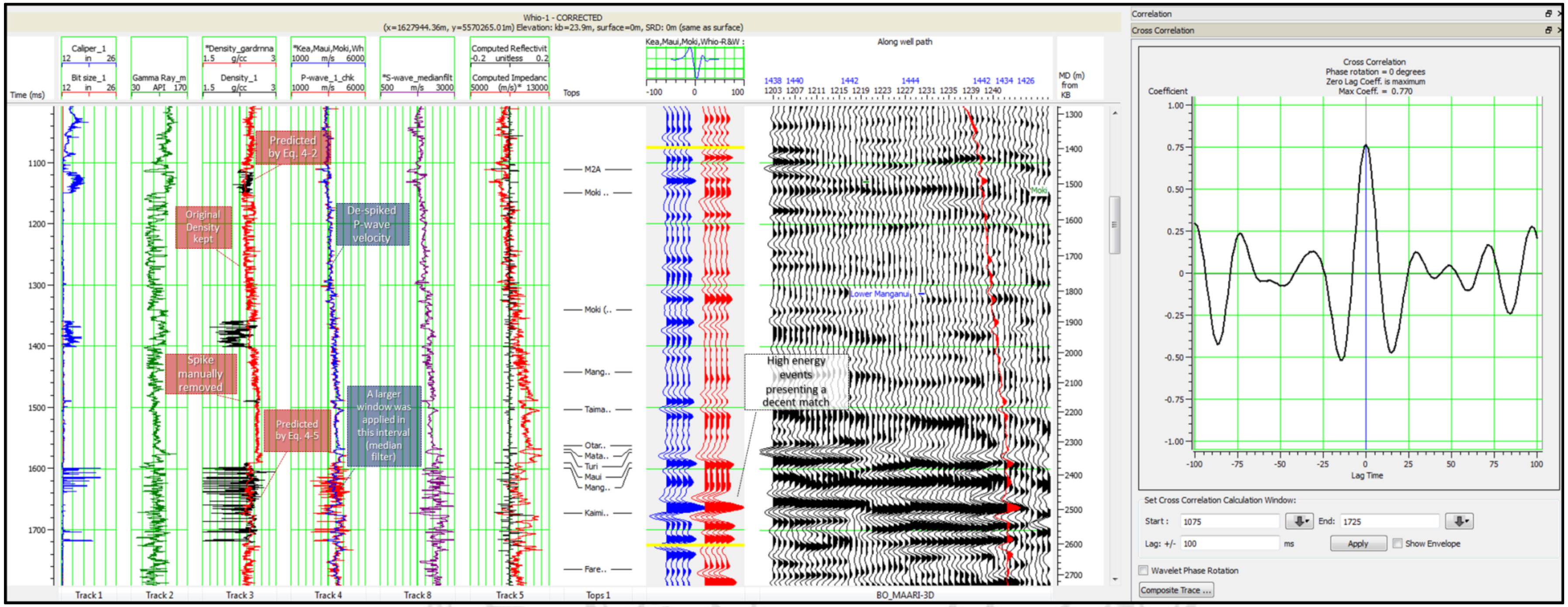

Figure 4.25: Seismic-to-well-tie in the deviated well Whio-1. Original and finals logs are presented. The final density (red curve, Track 3) and P-wave velocity (blue curve, Track 4) logs used to compute Impedance and reflectivity logs are assigned with an asterisk (*). Synthetic and actual seismic trace exhibit a good cross-correlation (77%) over the window 1075-1725 ms

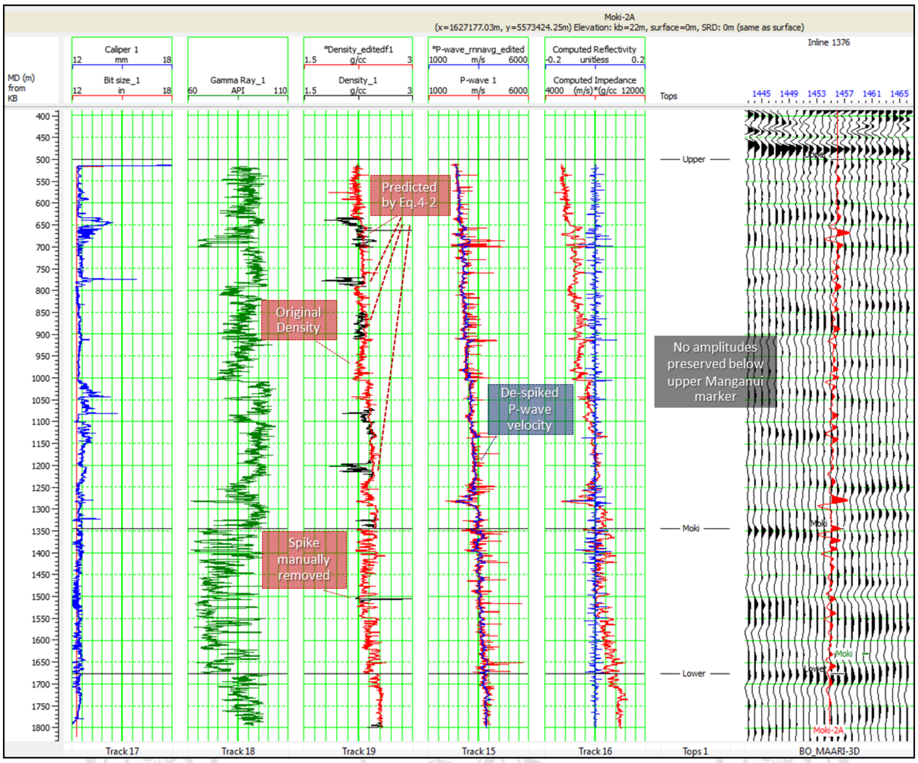

Figure 4.26: Well data from Moki-2A. Amplitudes possibly attenuated by a shallow gas event prevent the well from going through the seismic-to-well tie correlation

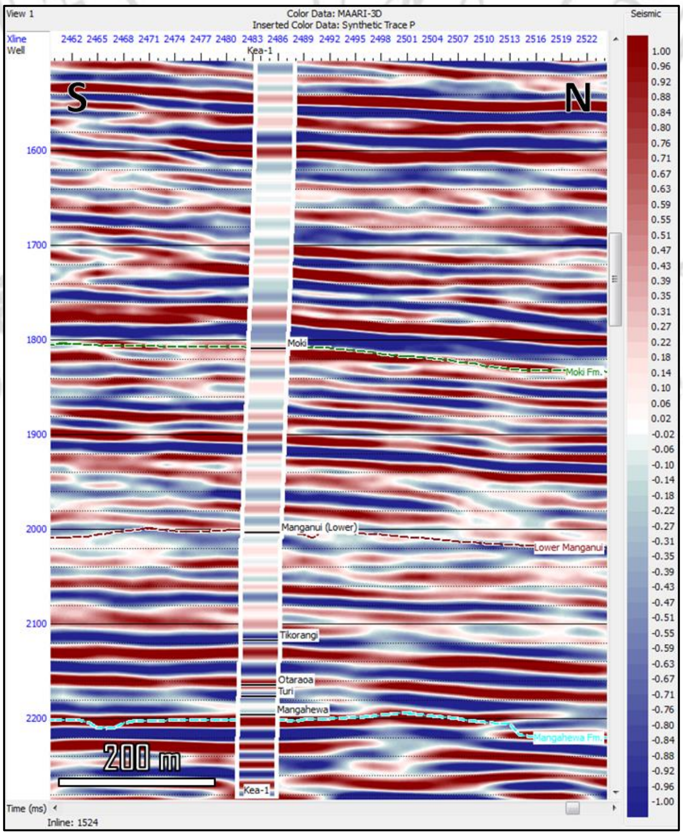

Figure 4.27: Colored synthetic trace for Kea-1 well displayed over seismic IL 1524

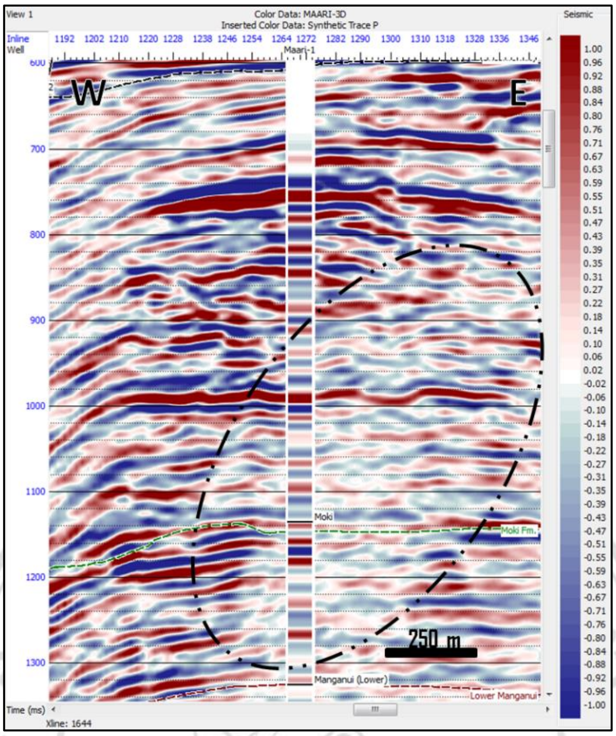

Figure 4.28: Colored synthetic trace for Maari-1 well displayed on Xline 1644. The black dashed ellipse highlights a zone where the amplitues are attenuated, restraining the correlation window analyzed due to a lack of significant events to correlate

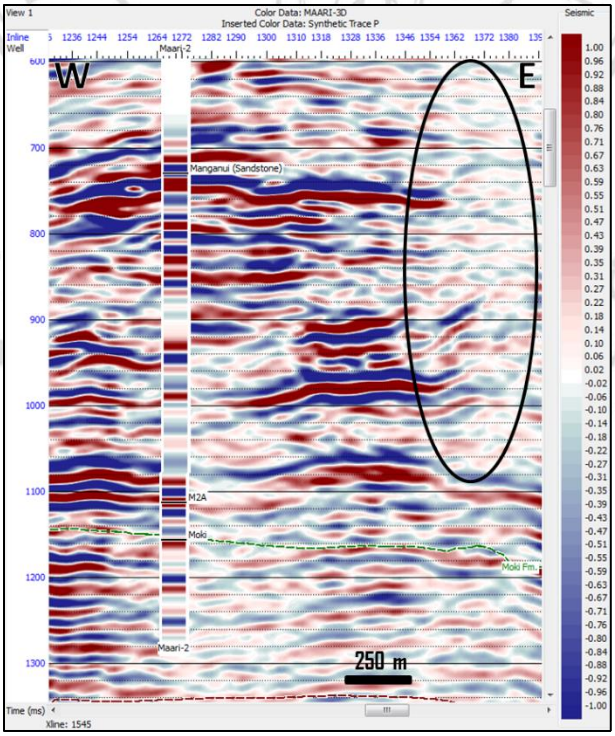

Figure 4.29: Colored synthetic trace for Maari-2 well displayed on Xline 1545. A possibly shallow gas anomaly attenuating amplitudes is highlighted by a black ellipse

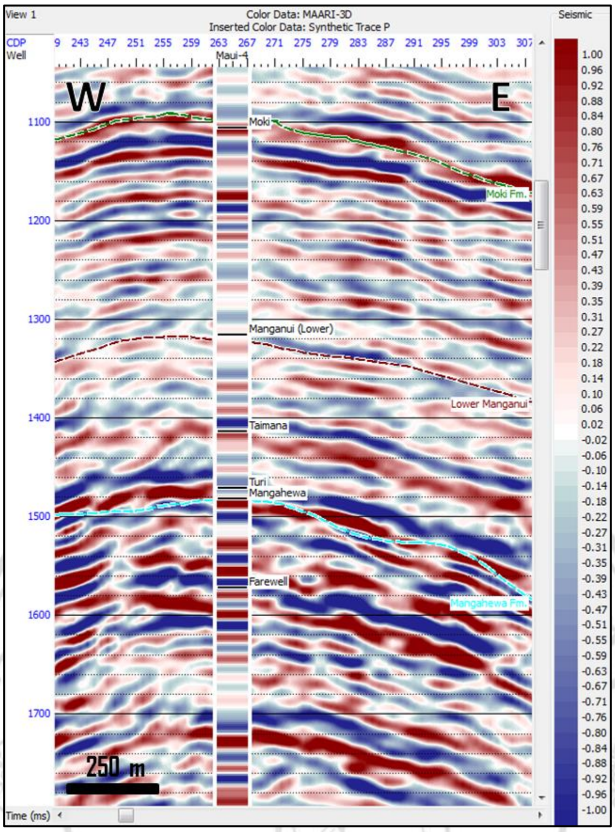

Figure 4.30: Colored synthetic trace for Maui-4 well displayed along an arbitrary line

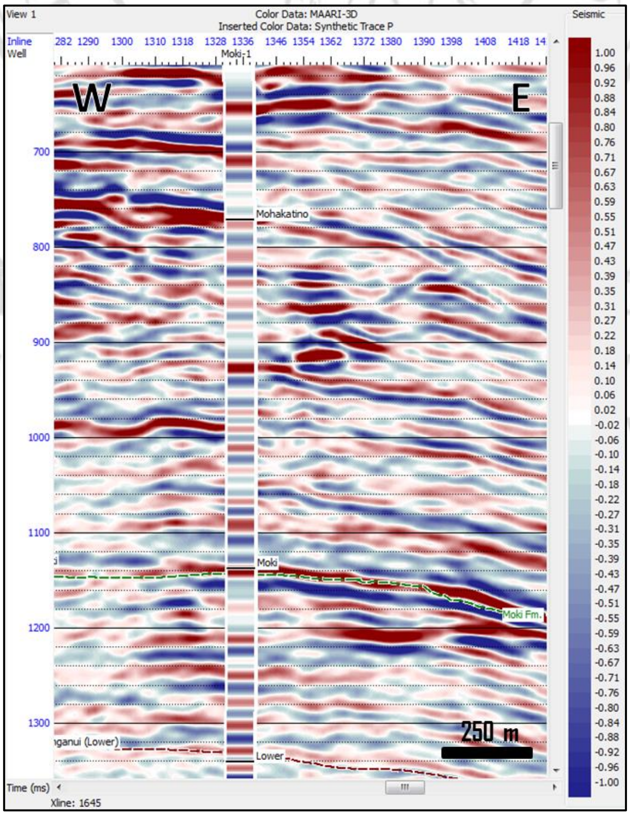

Figure 4.31: Colored synthetic trace for Moki-1 well displayed on seismic Xline 1645

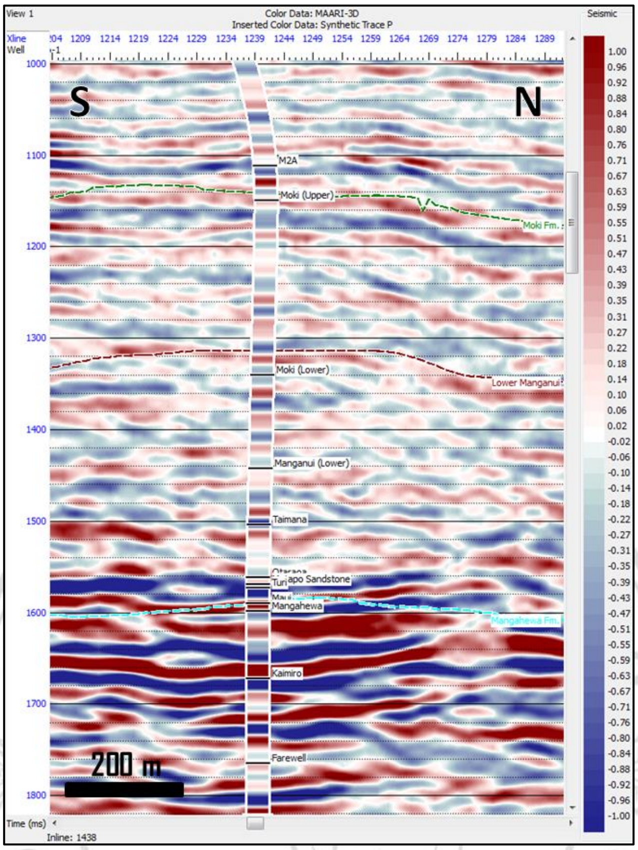

Figure 4.32: Colored synthetic trace for Whio-1 well displayed over seismic Inline 1438

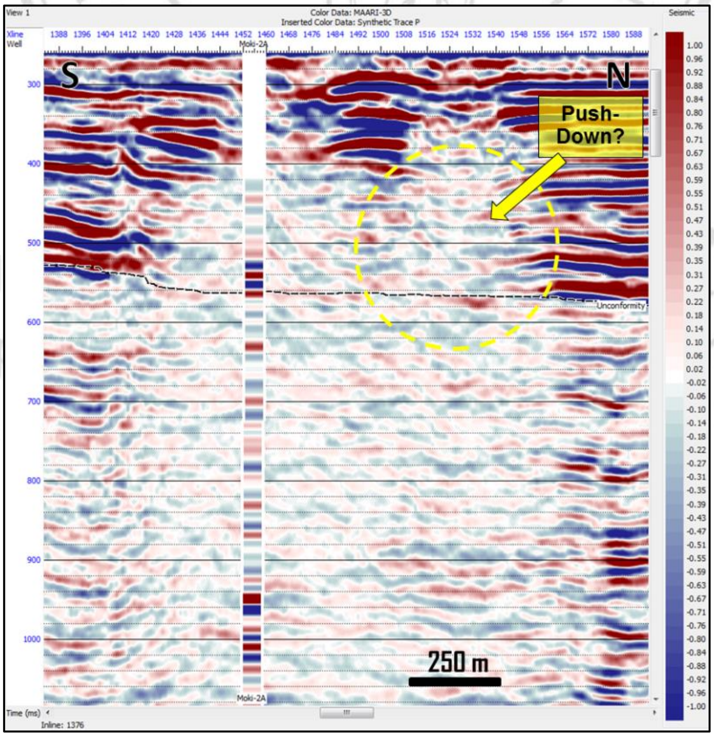

Figure 4.33: Well-tie for Moki-2A was incapacitated due to absorbed amplitudes, possibly caused by a shallow gas anomaly occurring at the well location (IL 1376)

4.3. Time-Depth Relationships

Located in the Southern Inversion Zone - Taranaki Basin, the Maari field is structurally complex. It presents high-angle faults and steeply dipping and folded structures, which are likely to cause significant lateral velocity variations throughout the Maari area. These variations are easily noticed if we plot the time-depth relationships (T:D charts) after tying six wells spread around the field. The following figures will present the computed average velocities (Vavg.), interval velocities (Figure 4.34) and T:D charts (Figure 4.35) for the wells Kea-1, Maari-1, Maari-2, Maui-4, Moki-1 and Whio-1. By analyzing the position of each well in the area, these plots can be fully understood. An arbitrary line crossing all these wells is shown in Figure 4.36.

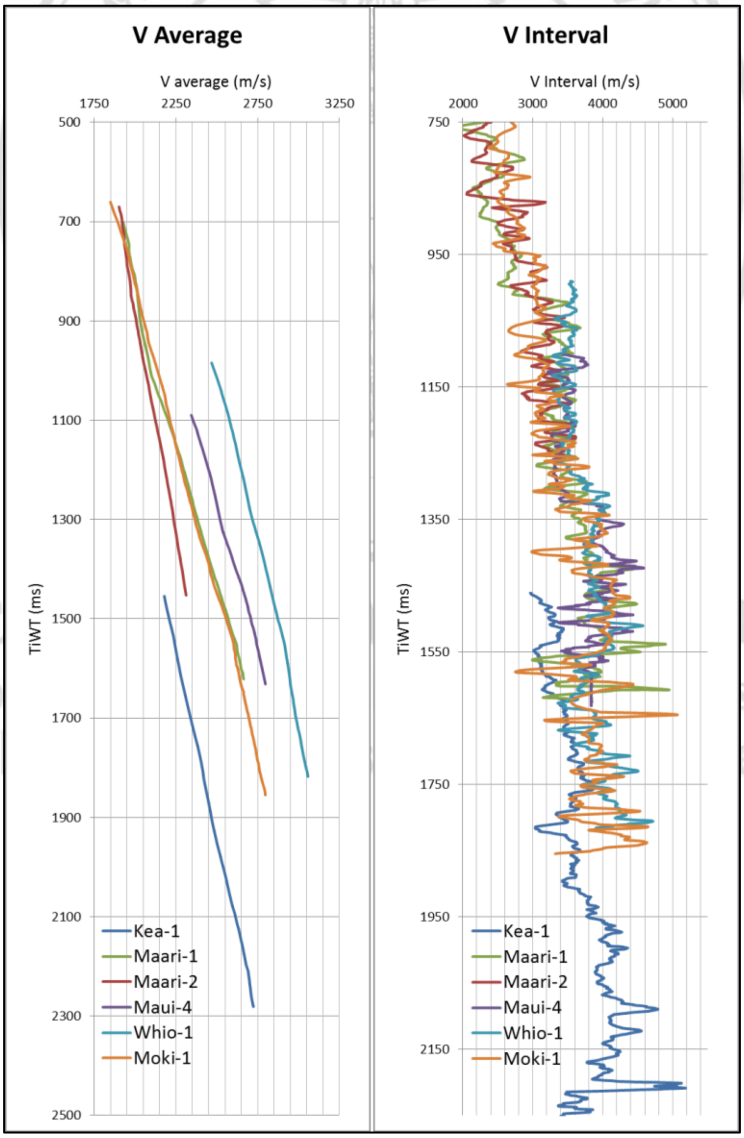

Figure 4.34: Calculated average and interval velocities after well-ties in the Maari area

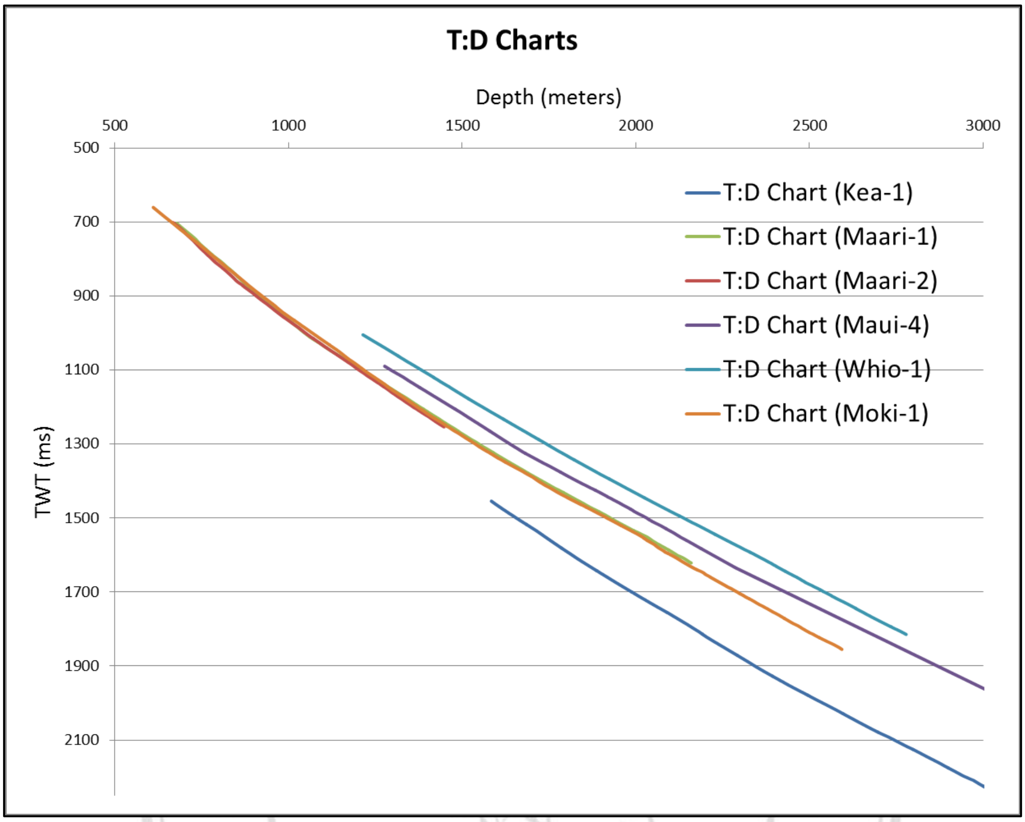

Figure 4.35: Time-Depth charts for each of the six wells: Kea-1, Maari-2, Maari-2, Maui-4, Whio-1 and Moki-1

One of the keys to understand the variations in the obtained time-depth relationships is the thickness of the young sediments, i.e. the sedimentary layers deposited after the Plio-Pleistocene unconformity (yellow horizon in Figure 4.36), at the location where the well was drilled. Take the well Kea-1, for example. It is located in the northern sector of the Maari area, where these young deposits have their thickest deposits. The young layers present considerably lower velocities than the older rocks below. Increasing depth of burial, compaction acts reducing porosity and consequently increasing density and p-wave velocity. So for this well, computed average velocity is lower than for all the other wells as shown in Figure 4.34. For the well Maui-4 and Whio-1, the opposite situation occurs. They are located where the young sediments have their thinnest deposits and below the Unconformity horizon are rocks that were uplifted by a reverse fault. Both wells cross the Unconformity horizon around 450 ms TWT. The older units were buried at greater depths than where they are located today, so higher velocities are expected. But the fact that along the Whio-1 well the highest average velocities are observed is interesting and not completely understood. An explanation would be if greater erosion had occurred where the Whio-1 well is located compared to the occurred at the Manaia structure, where Maui-4 is located. That would mean that the rocks located just below the unconformity at the Whio-1 well location had been buried at greater depths compared to the ones that are found in the Manaia structure. Consequently, the higher expected velocities for these rocks could explain what is observed in the average and interval velocity plots and also in the T:D relationships.

Unfortunately, the seismic imaging quality is damaged in the Maari field, as there are zones with dim amplitudes that do not allow a clear identification of events (lateral continuity, etc.) that could help to support this hypothesis. Also, the fact that the inversion produced asymmetrical structures and layers were folded without maintaining its original thicknesses make it difficult to be certain about why exactly higher average velocities are found along Whio-1. Another possible explanation is that this difference in average velocity could be due to the deviation in the Whio-1 well. Approximately 200 ms TWT of sonic velocity were measured with deviations up to 38°.

Finally, calculating and plotting average and interval velocities as well as observing the trends in the T:D chart is a manner of validating the well-ties. Figure 4.34 shows reasonable computed velocities, with some higher interval values associated to the Tikorangi limestone. All the time-depth relationships present a similar trend (Figure 4.36) and the differences are related to the thicknesses of recent deposits (above the Plio-Pleistocene unconformity) at the location of each well location, since this column of sediments is known to present significant slower velocities than rock units at greater depths.

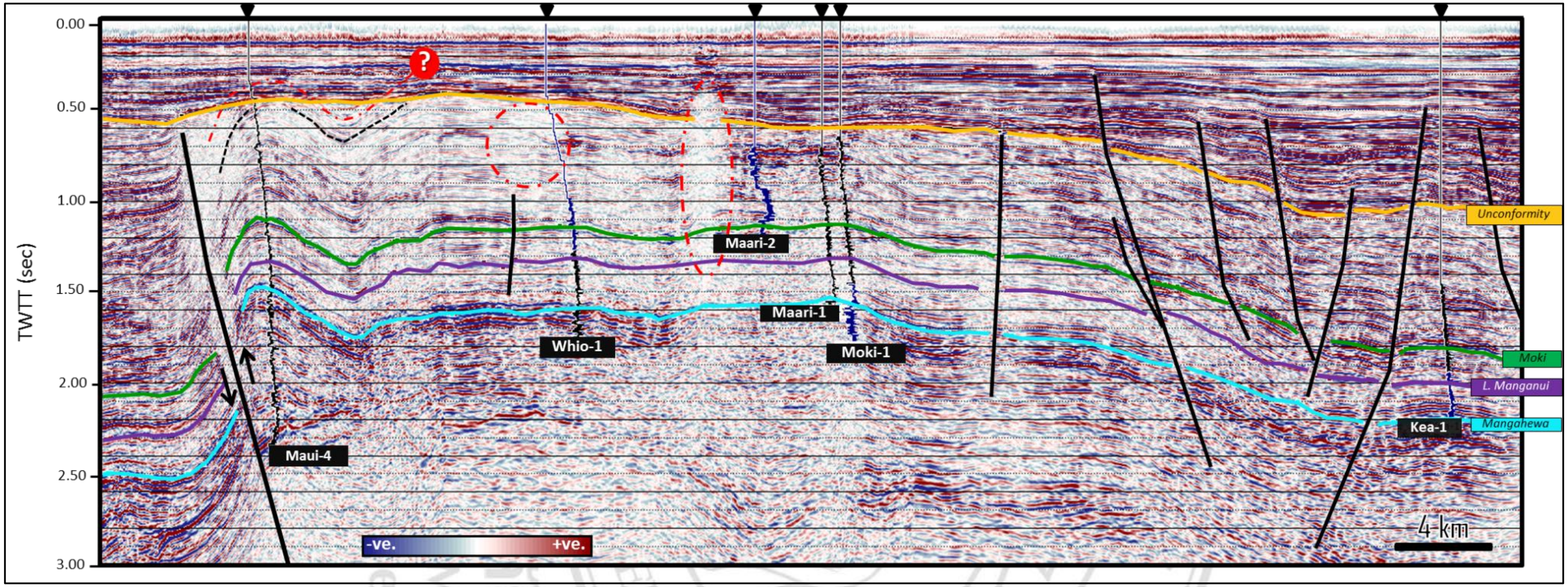

Figure 4.36: Arbitrary-line through all the tied wells. Red dashed areas show zones with attenuated amplitudes